Adipocyte-specific modulation of KLF14 expression in mice leads to sex-dependent impacts in adiposity and lipid metabolism

Running title: KLF14 is sex-dimorphic in mice metabolism

Qianyi Yang[1], Jameson Hinkle[1], Jordan N. Reed[1,2], Redouane Aherrahrou[1], Zhiwen Xu[3], Thurl E. Harris[4], Erin J. Stephenson[5], Kiran Musunuru[6,7,8], Susanna R. Keller[9], Mete Civelek[1,2]

[1]Center for Public Health Genomics, School of Medicine, University of Virginia, Charlottesville, VA 22908, USA.

[2]Department of Biomedical Engineering, School of Engineering and Applied Science, University of Virginia, Charlottesville, VA 22908, USA.

[3]Department of Chemistry, College of Arts and Sciences, University of Virginia, Charlottesville, VA 22908, USA.

[4]Department of Pharmacology, School of Medicine, University of Virginia, Charlottesville, VA 22908, USA.

[5]Department of Anatomy, College of Graduate Studies & Chicago College of Osteopathic Medicine, Midwestern University, Downers Grove, IL 60515, USA.

[6]Cardiovascular Institute, Perelman School of Medicine at the University of Pennsylvania, Philadelphia, PA, 19104, USA.

[7]Division of Cardiovascular Medicine, Department of Medicine, Perelman School of Medicine at the University of Pennsylvania, Philadelphia, PA, 19104, USA.

[8]Department of Genetics, Perelman School of Medicine at the University of Pennsylvania, Philadelphia, PA, 19104, USA.

[9]Division of Endocrinology and Metabolism, Department of Medicine, School of Medicine, University of Virginia, Charlottesville, VA, 22908, USA.

Corresponding authors:

Qianyi Yang, Ph.D. and Mete Civelek, PhD

University of Virginia

Center for Public Health Genomics

Old Med School 3836

PO Box 800717

Charlottesville, VA 22908-0717

Office Number: 434-243-1669

Fax Number: 434-982-1815

E-mail: qy5sy@virginia.edu and mete@virginia.edu

Word count: 6483

Number of tables: 2 (supplemental)

Number of figures: 8 main figures and 5 supplemental figures

ABSTRACT

Genome-wide association studies identified single nucleotide polymorphisms on chromosome 7 upstream of *KLF14* to be associated with metabolic syndrome traits and increased risk for Type 2 Diabetes (T2D). The associations were more significant in women than in men. The risk allele carriers expressed lower levels of the transcription factor KLF14 in adipose tissues than non-risk allele carriers. To investigate how adipocyte KLF14 regulates metabolic traits in a sex-dependent manner, we characterized high-fat diet fed male and female mice with adipocyte-specific *Klf14* deletion or overexpression. *Klf14* deletion resulted in increased fat mass in female mice and decreased fat mass in male mice. Female *Klf14*-deficient mice had overall smaller adipocytes in subcutaneous fat depots but larger adipocytes in parametrial depots, indicating a shift in lipid storage from subcutaneous to visceral fat depots. They had reduced metabolic rates and increased respiratory exchange ratios consistent with increased utilization of carbohydrates as an energy source. Fasting and isoproterenol-induced adipocyte lipolysis was defective in female *Klf14*-deficient mice and concomitantly adipocyte triglycerides lipase mRNA levels were downregulated. Female *Klf14*-deficient mice cleared blood triglyceride and NEFA less efficiently than wild type. Finally, adipocyte-specific overexpression of *Klf14* resulted in lower total body fat in female but not male mice. Taken together, consistent with human studies, adipocyte KLF14 deficiency in female but not in male mice causes increased adiposity and redistribution of lipid storage from subcutaneous to visceral adipose tissues. Increasing KLF14 abundance in adipocytes of females with obesity and T2D may provide a novel treatment option to alleviate metabolic abnormalities.

INTRODUCTION

Genome-Wide Association Studies (GWAS) identified several genetic variants on chromosome 7 upstream of the *KLF14* gene to be associated with a multitude of metabolic abnormalities, including insulin resistance, type 2 diabetes, and coronary artery disease (1–4). The associations were more pronounced in women than in men (5). GWAS of gene expression performed in the Multiple Tissue Human Expression Resource (MuTHER) and the Metabolic Syndrome in Men (METSIM) cohorts identified KLF14 as a master regulator of gene expression in subcutaneous adipose tissue, despite its nearly ubiquitously expression across all human tissues (6–9). GWAS-associated single nucleotide polymorphisms (SNPs) were also associated with KLF14 expression levels in *cis* and nearly 400 genes in *trans* in adipose tissue (1,6,10).The locus is one of the largest *trans*-eQTL hotspots known in the human genome (7). The results also suggested that disease-associated variants act in adipose tissue to increase disease risk. However, given that adipose tissue contains a multitude of cell types, it was not clear which cells were ultimately responsible for KLF14's adverse effects.

Several studies have implicated KLF14, a single exon gene in the Krüpple-like factor family of transcription factors, in the development of metabolic diseases, including obesity, insulin resistance, and T2D. Small *et al.* demonstrated that lowering KLF14 expression in preadipocytes from females prevented maturation to adipocytes as measured by the expression of adipogenesis markers and lipid accumulation (1). Histological analysis of subcutaneous adipose tissue biopsies showed that females who were homozygous for the T2D risk allele had larger adipocytes, suggesting that lower KLF14 expression is associated with adipocyte dysfunction (1). Collectively, these studies implied that KLF14 plays roles in adipogenesis and mature adipocyte size and function. T2D-associated variants also have strong associations with high density lipoprotein and triglyceride levels in the serum (11,12). However, the mechanisms by which KLF14 regulates adipocyte differentiation and function are not known.

To further investigate the role of KLF14 in adipocytes and to establish a mouse model that is relevant to humans, we characterized mice with adipocyte-specific *Klf14* deletion or overexpression. Our findings demonstrate that adipocyte KLF14 is a key regulator of lipid metabolism and, consistent with findings in

human, this regulation is female-specific. Our findings may facilitate the development of novel therapeutics to treat obesity and related metabolic diseases specifically in females.

MATERIALS and METHODS

Generation of mice with adipocyte-specific deletion and overexpression of *Klf14*

The generation of adipocyte-specific *Klf14* knockout mice has been described in detail elsewhere (1). Briefly, *in vitro* transcribed Cas9 mRNA, two gRNAs designed to target sites upstream and downstream of the *Klf14* gene locus, two single-strand DNA oligonucleotides bearing loxP sequences along with 80-nt homology arms matching the target sites were injected into the cytoplasm of fertilized oocytes from C57BL/6J mice (Supplementary Figure. 1A). Genomic DNA samples from founders were screened for correct loxP sequences flanking the *Klf14* gene by PCR and confirmed by Sanger sequencing. Mice with two loxP sites that segregated on the same chromosome were bred with *Adipoq*-Cre mice on the C57BL/6J background [B6; FVB-Tg (*Adipoq*-Cre)1Evdr/J, The Jackson Laboratory] to obtain litters with homozygous *Klf14* loxP knock-in mice that were Cre+ ($Klf14^{fl/fl}$*Adipoq*-Cre+ or KO) and wild type mice that were positive for *Klf14* loxP but negative for *Adipoq*-Cre ($Klf14^{fl/fl}$*Adipoq*-Cre- or WT) for experiments. The presence of the *Adipoq*-Cre allele was confirmed by PCR (Supplementary Table 1). Absence of KLF14 protein expression in adipocytes isolated from knockout animals was confirmed by Western Blotting (Supplementary Figure 1B). To generate mice with adipocyte-specific overexpression (OE) of *Klf14*, *Klf14* was PCR amplified from C57BL/6J cDNA and cloned downstream of the 5.43 Kb Adiponectin (*Adipoq*) promoter at an EcoRV site using Gibson Assembly into the pADNpcDNA3.1 KanR vector. The 8.2 Kb expression cassette containing the *Adipoq* promoter, *Klf14* cDNA, and 3' UTR was gel purified after restriction digestion with NotI and NgoMIV. The transgene was injected into pronuclei of fertilized C57BL/6N eggs to produce random integrants at the University of California, Irvine Transgenic Mouse Facility. The presence of the transgene was confirmed by PCR (Primers are listed in Supplementary Table 1). We labeled these mice *Adipoq-Klf14*-OE. Increased KLF14 protein expression in adipocytes isolated from transgenic animals was confirmed by Western Blotting (Supplementary Figure 1C).

Animal Husbandry

All animal protocols were approved by the University of Virginia Animal Care and Use Committee. Mice were maintained in a 12-hour light/12-hour dark cycle with free access to water and standard chow (Envigo Teklad LM-485 irradiated mouse/rat sterilizable diet. Cat No. 7912). For high fat diet (HFD) studies, the mice were fed a rodent diet with 40% Kcal fat, 43% Kcal carbohydrate and 17% Kcal protein (Research Diets, Inc., Cat No. D12079B). The mice were euthanized by cervical dislocation after induction of deep anesthesia using isoflurane, consistent with the recommendations of the Panel of the American Veterinary Medical Association.

Body composition analysis

Total body fat and lean mass were assessed in conscious mice using a noninvasive quantitative magnetic resonance imaging system (Echo Medical Systems, Cat No. EchoMRI™ 3-in-1 v2.1;), as previously reported (13).

Glucose and insulin tolerance tests

Glucose and insulin tolerance tests were performed as previously described (14). For the glucose tolerance test, mice were fasted from 7 AM to 1 PM and were administered glucose at 1 mg/g body weight intraperitoneally. Blood glucose levels were measured with a OneTouch Ultra Glucometer (Lifescan) in blood drops obtained from nicked tail veins before and at 10, 20, 30, 60, 90 and 120 min after the injection. The insulin tolerance test was performed at 1–2 PM on mice fed ad libitum. Insulin (Humulin, 100 U/ml, from Eli Lilly) at 0.75 U/kg body weight was administered by intraperitoneal injection of a 0.25 U/ml solution in 0.9% NaCl. Blood glucose levels were measured immediately before and at 15, 30, 45, 60, and 90 min after the injection.

Plasma insulin and lipid analysis

Mice were either fed ad libitum, and samples taken between 7 AM and 8 AM, or they were fasted for 6 hours from 7 AM to 1 PM before samples were taken. Whether measurements were done in the fed or fasted state is indicated in the Results section. For insulin, fatty acids, and glycerol measurements, blood samples were collected either through retro-orbital bleeding or cardiac puncture. For insulin, high density lipoprotein (HDL),

total cholesterol, and triglyceride (TG) measurements, plasma was obtained from the blood by the addition of heparin at 10 U/ml, followed by centrifugation at 7800 rcf in a microfuge for 10 min at 4°C. Insulin levels were measured with an ELISA (Alpco, Cat No. 80-INSMSU-E01). Total cholesterol, HDL, and TG levels were measured using colorimetric assays (FUJIFILM Wako Diagnostics, Cat Nos. 999-02601, 997-72591, 464-01601).

Indirect calorimetry analysis

For determination of energy expenditure and respiratory exchange ratios, mice were placed in Oxymax metabolic chambers (Columbus Instruments), under a constant environmental temperature (22 °C) and a 12-hour light, 12-hour dark cycle as previously described (15). Oxygen consumption (V_{O2}), carbon dioxide production (V_{CO2}), and ambulatory activity were determined for each mouse every 15 min over a 72-h period. Experimental mice were acclimated to the cages during the first 24 hours. Measurements taken during the following 48 hours were used for data analysis. Respiratory exchange ratios (RER) were calculated as carbon dioxide production/oxygen consumption (V_{CO2}/V_{O2}). Carbohydrate utilization was calculated as (20 kJ/L × V_{O2} uptake) × [(RER - 0.7)/0.3] and fat utilization was calculated as (20kJ/ × V_{O2}uptake) × (1 - [(RER × 0.7)/0.3)] (16). Both body fat and lean mass were included as covariates in the models used to analyze data obtained from the CLAMS experiments. Mice in each chamber had free access to water and food. Locomotor activity was monitored by a multidimensional infrared light beam system surrounding each cage.

***In vivo* lipolysis**

To determine lipolysis *in vivo*, two different experiments were performed. For lipolysis under fasting condition, blood samples were drawn from tail veins of 24-week-old mice using non-heparinized glass capillary tubes at 5 PM before food was withdrawn and 9 AM after 16-hour fasting to measure non-esterified fatty acids (NEFA) and glycerol. For β-adrenergic receptor stimulation experiments, blood samples were drawn from tail veins of random-fed 25-week-old mice via non-heparinized glass capillary tubes before stimulation. After a short recovery period (30 minutes), mice were injected intraperitoneally with 10 mg/kg isoproterenol (prepared in

saline; Sigma Aldrich Cat No I6504). A second blood sample was collected 15 min post-injection. Blood from non-heparinized capillary tubes was allowed to clot on ice before centrifugation at 500 g for 20 min at 4 °C. Glycerol and NEFA concentrations in serum were determined colorimetrically using commercially available reagents (Sigma Aldrich, Cat No. F6428, Wako Life Sciences, Inc., Cat No. NEFA-HR (2)).

In vivo lipid challenge

Experimental mice were fasted for 4 hours before the test (7 –11 AM). Olive oil (6 µl/g body weight) was given by oral gavage as described previously (17). Blood samples were drawn via heparinized (for TG)/non-heparinized (for NEFA) capillary tubes from tail veins before (time 0) and at 1, 2, 3, and 4 hours after gavage. TG and NEFA measurements were performed as described above.

Determination of adipocyte sizes

Subcutaneous white adipose tissue (WAT) and parametrial-periovarian/epidydimal WAT from four mice of each sex and genotype were excised and fixed in 10% neutral buffered formalin (18). Tissues were embedded in paraffin, and 5 µm thick sections were prepared and stained with hematoxylin and eosin (H&E) at the University of Virginia Research Histology Core. Slides were scanned and images were acquired with an EVOS microscope camera. Quantification of adipocyte size was done using ImageJ (version 1.48) (19). Images were processed as described previously (20).

Sex hormone measurements

Mouse sera collected at the time of euthanasia were stored at −80°C. After thawing, they were allowed to equilibrate at room temperature and spun to remove aggregates. 100 µL of 1:10 diluted sera per well were aliquoted for enzyme-linked immunosorbent assays (ELISA) in 96-well plates. Free testosterone, progesterone and estradiol levels were measured using Testosterone Parameter assay kit (R&D Systems, Cat No. KGE010), Progesterone ELISA Kit (Cayman Chemical, Cat No. 582601) and Estradiol ELISA Kit (Cayman Chemical, Cat No. 501890) following manufacturers' instructions (21).

Primary mouse adipocyte isolation

Adipocytes were isolated from subcutaneous and parametrial-periovarian/epididymal WAT as previously described (22). Immediately after euthanization fat pads were removed, placed in Krebs Ringer HEPES (KRH)–BSA buffer containing collagenase type I (Worthington Biochemical Corp., 1 mg/ml, 2 mg/g of tissue) and minced with scissors. Small tissue pieces were incubated in a 37°C shaking water bath (100 rpm) for 1 hour. Fat cells were separated from non-fat cells and undigested debris by filtration through a 0.4 mm Nitex nylon mesh (Tetko) and four washes by flotation with KRH buffer without BSA. After centrifugation at 1000 g for 15 minutes at 4°C the isolated fat cells floating on the surface were used for total RNA extraction and preparation of cell lysates for immunoblotting.

Total RNA extraction, cDNA synthesis and real-time PCR

Total RNA was isolated from parametrial-periovarian/epididymal and subcutaneous adipocytes using a combination of Trizol Reagent® (Thermo fisher Scientific, USA) and miRNeasy kit (Qiagen, Germany) according to the manufacturers' instructions (23). Adipocytes isolated from 200 mg of tissue in the previous step were homogenized in 2 ml of Trizol Reagent® using tissue-tearor homogenizer (Model 985370, BioSpec Products, Inc). After homogenization, samples were incubated at room temperature for 5 minutes and centrifuged at 12,000 g for 10 min at 4°C. The resulting fat monolayer on top was carefully avoided when pipetting the rest of the sample into a clean tube. 400 µl of chloroform was then added and samples mixed by vortexing. Samples were kept at room temperature for 3 minutes before centrifugation at 12,000 g for 30 min at 4°C. After centrifugation, samples separated into three phases with the RNA in the upper phase. The RNA phase was transferred to a new tube without disturbing the interphase. Sample volumes were measured and 1.5x sample volumes of 100% ethanol added. Samples were mixed thoroughly by inverting tubes several times. Samples were then loaded on miRNeasy spin columns (Qiagen) and the manufacturer’s protocol was followed for subsequent steps. Total RNA was eluted in 30 µl of RNAse-free water. Total RNA concentrations were quantified using a Qubit Fluorometer and a Qubit RNA BR assay kit (Thermo Fisher Scientific). 1 µg of total RNA was reverse transcribed using SuperScript IV reverse transcriptase (Invitrogen). Real-time PCR was

performed in the QuantStudio™ 5 Real-Time PCR System (ThermoFisher Scientific) using SYBR Green Master Mix (Roche) and gene-specific primers (Supplementary Table 2).

Protein extraction and Western blotting

Total protein was extracted from cells or tissues using cell lysis buffer (Cell Signaling, Cat No. 9803), containing 20 mM Tris-HCl (pH 7.5), 150 mM NaCl, 1 mM Na_2EDTA, 1 mM EGTA, 1% Triton, 2.5 mM sodium pyrophosphate, 1 mM beta-glycerophosphate, 1 mM Na_3VO_4, and 1 µg/ml leupeptin. Protease inhibitor cocktail (ThermoFisher Scientific) and phosphatase inhibitor (ThermoFisher Scientific) were added to the lysis buffer before extraction. Protein concentrations were determined using a Pierce BCA Protein Assay Reagent (Pierce Biotechnology). Proteins (10 ug protein/lane) were separated by SDS-PAGE. Electrophoresis was conducted using a Xcell II mini cell with 4-12% NuPAGE Tris-acetate gradient SDS-polyacrylamide gels. Protein samples were transferred onto polyvinylidene difluoride membranes using an Xcell II Blot Module (Invitrogen). The membranes were blocked in Intercept® (TBS) blocking buffer (Licor Inc.) for 1 hour at room temperature, and probed with primary antibody in 0.1% Tween LiCor blocking buffer overnight at 4°C. The KLF14 antibody was a gift from Dr. Roger D. Cox (MRC Harwell Institute). It was generated at Eurogentec by immunizing rabbits against the C-DMIEYRGRRRTPRIDP-N peptide. Full length purified KLF14 purchased from Creative Biomart (Cat No. KLF14-481H) served as positive control. The β-actin antibody was from Cell Signaling Technology (Cat No. 3700s). The membranes were washed twice for 10 min each in TBS-0.01% Tween buffer solution and then probed with IR-Dye labeled secondary antibodies (926-32211 and 926-68072) in 0.1% Tween, 0.01% SDS LiCor blocking buffer for 1 hour at room temperature. Several washes in TBS-0.01% Tween buffer solution were repeated after labeling with secondary antibodies. The blots were scanned using the LiCor laser-based image detection method.

Statistical analysis

Trial experiments were used to determine sample size with adequate statistical power. Measurement values that were beyond the boundary determined by the interquartile range were considered outliers and were excluded

from statistical analyses. Since the scatter of the data follows normal distribution, all analyses were conducted with Student's *t*-test with a two-tail distribution. Comparisons with *P* values <0.05 were considered significant. Effect size (β) was calculated by subtracting the mean difference between two groups, and dividing the result by the pooled standard deviation. $\beta = (M_2 - M_1) / SD_{pooled}$, $SD_{pooled} = \sqrt{((SD_1^2 + SD_2^2) / 2)}$; where M is the mean and SD is the standard deviation.

RESULTS

Adipocyte-specific deletion of KLF14 modifies adiposity, and insulin and lipid levels in female mice

Adipocyte-specific *Klf14* knockout (*Klf14*$^{fl/fl}$*Adipoq*-Cre+ or KO) mice were born at expected Mendelian ratios and were indistinguishable from wildtype (*Klf14*$^{fl/fl}$*Adipoq*-Cre- or WT) littermates at birth. At 8 weeks of age mice were placed on a 45% high fat (HF) diet (Research Diets D12079B). We measured body weights over a 12-week period (Figure 1A). Female *Klf14*$^{fl/fl}$*Adipoq*-Cre+ mice showed similar body weight increases as WT littermates. However, male *Klf14*-deficient mice had lower body weight starting at 8 weeks on the HF diet (with 8% difference after 12 weeks on HF diet, P=0.018) (Figure 1B, left). In humans, lower KLF14 expression is associated with higher visceral fat mass (1). To determine whether loss of KLF14 in adipocytes affected adiposity on the HF diet, we measured body composition using EchoMRI (Figure 1A). We found increased fat mass relative to lean mass in female *Klf14*$^{fl/fl}$*Adipoq*-Cre+ mice, while in male mice we observed the opposite (Figure 1B, middle and right). When determining individual organ weights normalized to tibia length, we found no differences between WT and *Klf14*-deficient mice for most organs, including brain, heart, kidney, muscle, spleen, and pancreas (Supplementary Figure 2). However, we observed that parametrial-periovarian fat depots in female *Klf14*-deficient mice were 70% larger ($\beta_{perigonadal}$=1.105, $P_{perigonadal}$=0.02), whereas subcutaneous and epididymal fat depots of male *Klf14*-deficient mice were 33% and 27% smaller compared to WT littermates (β_{subq}=-1.073, P_{subq}=0.01; $\beta_{epididymal}$=-1.006, $P_{epididymal}$=0.01) (Figure 1C). Notably, adipocyte *Klf14* deficiency resulted in decreased liver weight in males and a trend towards a decrease in females (β_{male}=-0.626, P_{male}=0.05; β_{female}=-0.639, P_{female}=0.18) (Figure 1C).

In humans, lower KLF14 expression in adipose tissue is associated with higher serum insulin and lower HDL levels with a stronger effect in females (1). Consistent with this, we observed 78% higher insulin and 25% lower HDL levels in *Klf14*-deficient female but not in male mice after a 6h fast (Figure 1D and E, $\beta_{female,insulin}$=0.947, $P_{female,insulin}$=0.036; $\beta_{female,HDL}$=1.352, $P_{female,HDL}$=0.004). Total cholesterol and non-esterified free fatty acids (NEFA) were lower by 19% and 26% while triglyceride (TG) levels were 10% higher in female mice with *Klf14* deficiency in adipocytes (Figure 1F, G and H, $\beta_{female,cholesterol}$=1.176, $P_{female,cholesterol}$=0.011;

$\beta_{female,NEFA}$=1.173, $P_{female,NEFA}$=0.031, $\beta_{female,TG}$=1.250, $P_{female,TG}$=0.044). Mutant male mice also had lower NEFA levels (Figure 1G, $\beta_{male,NEFA}$=1.022, $P_{male,NEFA}$=0.01) but normal serum cholesterol and TG levels (Figure 1F and H).

Adipocyte-specific deletion of KLF14 affects adipocyte size

The parametrial-periovarian fat depot in female mice and the epididymal fat depot in male mice are considered visceral fat. Larger visceral fat depots with bigger adipocytes are a significant risk factor for T2D, cardiovascular disease, and hypertension (24,25). Adipocyte size is increased in obese conditions (26,27). To test if adipocyte size was altered as a result of *Klf14* deficiency, we performed histological analysis using hematoxylin and eosin (H&E) staining of subcutaneous and perigonadal fat depots (Figure 2A). We observed that female mice with adipocyte deletion of *Klf14* had 25% smaller adipocytes in the subcutaneous depot (β_{subq}=-0.422, P_{subq}=4.02 × 10^{-85}) and 70% larger adipocytes in the parametrial-periovarian depot relative to WT mice ($\beta_{periovarian}$=0.706, $P_{periovarian}$=2.25 × 10^{-175}) (Figure 2B). In contrast, male mice with adipocyte deletion of *Klf14* had 6% larger adipocytes in the subcutaneous depot (β_{subq}=0.09, P_{subq}=1.66 × 10^{-3}) and 14% smaller adipocytes in the epididymal depot relative to WT mice ($\beta_{epididymal}$=-0.233, $P_{epidiymal}$=2.66 × 10^{-15}) (Figure 2B). These findings suggest that KLF14 regulates adipocyte size and adipose tissue mass in a depot specific and sex specific manner.

Deletion of KLF14 in adipocytes causes increased insulin resistance in female mice

Adipose tissues regulate systemic glucose metabolism and insulin sensitivity (28,29). Genetic studies showed that T2D risk alleles associated with lower KLF14 expression in adipose tissue led to higher fasting insulin in humans indicating decreased insulin sensitivity (1,5). As described above, we also observed increased insulin levels in female *Klf14*-deficient mice (Figure 1D). To further explore whether the differences in adipose tissue mass as a result of *Klf14* deletion in adipocytes affected systemic glucose homeostasis and insulin sensitivity, we performed glucose and insulin tolerance tests with intraperitoneal injections of glucose or insulin after 7 and 9 weeks of HF diet, respectively. Mice with adipocyte-specific *Klf14* deletion had a similar response to an

intraperitoneal glucose bolus as WT littermates (Figure 3A). However, in the insulin tolerance test female mice with adipocyte-specific *Klf14* deletion displayed increased glucose levels compared to WT littermates with 19% higher calculated area under the curve (AUC) (β_{AUC}=1.233, P_{AUC}=0.005) (Figure 3B) indicating increased insulin resistance. Insulin sensitivity for male mutant mice was similar to WT (β_{AUC}=0.027, P_{AUC}=0.943) (Figure 3B).

Deletion of KLF14 in adipocytes modifies energy metabolism in female mice

Increased fat mass in female mice with *Kl14* deficiency suggested a defect in energy balance. To investigate the role of KLF14 in energy homeostasis, we performed indirect calorimetry studies using metabolic cages. Food consumption was comparable between *Klf14*-deficient and WT mice (Supplementary Figure 4), and mice of both genotypes maintained body weights within 5-10% of their initial weight during the three-day period in the metabolic cages. Despite these similarities, female *Klf14*$^{fl/fl}$*Adipoq*-Cre+ mice showed a 38% decrease in locomotor activity ($\beta_{\text{Locomotor activity}}$=2.212, $P_{\text{Locomotor activity}}$=5.2 × 10^{-4}) compared to WT mice during the dark cycle (Figure 4A). Oxygen consumption (VO_2) was lower in both the light and dark cycles by 26% and 19%, respectively ($\beta_{O2,\ dark}$=2.320, $P_{O2,\ dark}$=0.003; $\beta_{O2,\ light}$=1.569, $P_{O2,\ light}$=0.0095) while CO_2 release was 14% lower in the light cycle and trended towards a decrease in the dark cycle ($\beta_{CO2,\ dark}$=0.900, $P_{CO2,\ dark}$=0.093; $\beta_{CO2,\ light}$=1.262, $P_{CO2,\ light}$=0.026) (Figures 4B and C). The calculated respiratory exchange ratio ($RER=\dot{V}_{CO2}/\dot{V}_{O2}$), an indicator for the metabolic energy source (carbohydrate or fat), was higher (close to 1) for female *Klf14*$^{fl/fl}$*Adipoq*-Cre+ mice than for WT littermates ($\beta_{RER,dark}$=4.258, $P_{RER,dark}$=1.0 × 10^{-6}) in the dark cycle (Figure 4D), suggesting predominant use of carbohydrates as energy source, despite being fed a HF diet. The indirect calorimetry measurements allowed us to estimate consumed substrates using gas exchange ratios as a surrogate for substrate utilization (16). Female *Klf14*$^{fl/fl}$*Adipoq*-Cre+ mice had 82% higher carbohydrate utilization ($\beta_{carbohydate,dark}$=2.015, $P_{carbohydrate,dark}$=0.01) and 79% decreased fat utilization ($\beta_{fat,dark}$=-5.400, $P_{fat,dark}$=1.1 × 10^{-6}) in the dark cycle compared to WT mice. We did not observe differences for any of the measured parameters for male mice in dark or light cycles (Figure 4).

Deletion of KLF14 in adipocytes causes defects in lipid metabolism in female mice

We reasoned that defects in lipid breakdown (lipolysis) or lipid uptake and synthesis (lipogenesis) in adipocytes could explain the shift in energy source for female mice. Compatible with these possibilities, circulating NEFA and triglyceride levels were decreased and increased under fasting conditions, respectively, in female mutant mice (Figures 1G and H). To follow up on these changes, we first measured lipolytic products, non-esterified fatty acids (NEFA) and glycerol, after 16 hours of fasting. NEFA levels increased as a result of fasting, as expected (Figure 5A). However, female *Klf14*$^{fl/fl}$*Adipoq*-Cre+ mice had 17% and 38% lower NEFA levels compared to WT littermates in fed and fasted states (β_{fed}=-1.416, P_{fed}=0.013; β_{fasted}=-3.231, P_{fasted}=1 × 10^{-4}) (Figure 5A) with NEFA levels in *Klf14*-deficient female mice increasing to a lesser extent compared to WT littermates in response to fasting (β=-1.292, *P*=0.021) (Figure 5B). Glycerol in female mice was only decreased in the fed state (β_{fed}=2.157, P_{fed}=7 × 10^{-4}) (Figure 5C and D). No differences in NEFA and glycerol were observed in male mice except that NEFA under fed conditions were slightly increased (p=0.036) (Figure 5).

Adipocyte lipolysis is regulated by hormonal and neuronal stimulation (30) with beta-adrenergic receptor signaling potently increasing lipolysis (31). To further corroborate that female adipocyte *Klf14*-deficient mice indeed had a defect in lipolysis, we thus quantified serum levels of NEFA and glycerol in response to isoproterenol that stimulates beta-1 and beta-2 adrenergic receptors (32).Female *Klf14*$^{fl/fl}$*Adipoq*-Cre+ mice had 21% and 22% lower NEFA levels compared to WT littermates under fed condition in non-stimulated and stimulated states, respectively ($\beta_{non\text{-}stimulation}$=-2.692, $P_{non\text{-}stimulation}$= 9 × 10^{-5}; $\beta_{stimulated}$=-2.699, $P_{stimulated}$ = 8 × 10^{-5}) (Figure 5E) with NEFA levels in *Klf14*-deficient female mice increasing to a lesser extent than in WT littermates in response to stimulation (β=-1.022, *P*=0.06) (Figure 5F). No differences were observed in male mice (Figure 5E and F). Similar to fasting experiments, we observed a difference in serum glycerol level in female mice before stimulation (β_{female}=-0.307, P_{female} = 0.021) but not after (β_{female}=-0.301, P_{female} = 0.559) (Figure 5G). Changes in serum glycerol levels upon stimulation did not differ between genotypes in both female or male mice (β_{female}=0.815, P_{female} = 0.166; β_{male}=-0.031, P_{male} = 0.951) (Figure 5H). The difference in NEFA and glycerol responses to induced lipolysis is most likely due to different metabolic fates of NEFA and glycerol after release into circulation.

TG hydrolysis to NEFA and glycerol is achieved in a three-step enzymatic pathway (Figure 5I). We measured the expression of adipocyte triglyceride lipase (ATGL), the first enzyme in the TG breakdown pathway and found that mRNA levels of *Pnpla2* in adipocytes isolated from subcutaneous and parametrial-periovarian/epididymal fat were decreased by 24% and 29%, respectively, in female mice as a result of *Klf14* deficiency (β_{sWAT}=-9.320, $P_{sWAT}=5 \times 10^{-3}$; β_{pWAT}=-13.139, $P_{pWAT}=1 \times 10^{-4}$) (Figure 5J), but were normal in male mice. We also measured hormone sensitive lipase (HSL), the second enzyme in the TG breakdown pathway, but did not observe differences in *Lipe* mRNA expression in adipocytes of male or female mice (Figure 5K), which may be due to the fact that HSL activity is predominantly regulated by phosphorylation (33). Lower *Pnpla2* expression is consistent with above-described decreased lipolysis and increased fat mass and adipocyte size of visceral adipocytes in female mutant mice. Visceral adipocytes are normally more lipolytically active when compared to subcutaneous adipocytes (34).

Our metabolic cage data indicated that female *Klf14*$^{fl/fl}$*Adipoq*-Cre+ mice were not able to efficiently use dietary fatty acids leading us to speculate that there was also a defect in lipid uptake. Therefore, we challenged mice with a bolus of olive oil by oral gavage and measured TG and NEFA levels to quantify lipid clearance from the bloodstream. We observed that blood TG and NEFA clearance were both decreased in female mutant mice compared to WT mice ($\beta_{4hr\text{-}TG}$=4.610, $P_{4hr\text{-}TG}=7.2 \times 10^{-9}$; $\beta_{4hr\text{-}NEFA}$=3.528, $P_{4hr\text{-}NEFA}=8 \times 10^{-6}$) (Figure 6A and B), consistent with decreased use of lipids as an energy source in female *Klf14*-deficient mice. No differences were observed in male mice (Figure 6C and D). These results are consistent with our metabolic cage data that female mice use less fat as their energy source.

Uptake of fatty acids into cells is achieved predominantly via a saturable protein-facilitated process (35) (Figure 5I). Several proteins facilitate the uptake of fatty acids, among which the best characterized are CD36, FABPs and FATPs (36–38). Fatty acids are also synthesized in cells through *de novo* lipogenesis that is catalyzed by ATP-citrate lyase (encoded by *Acly*) (39), acetyl-CoA carboxylase (encoded by *Acaca* and *Acacb*) (40), and fatty acid synthase (encoded by *Fasn*) (41). Fatty acids are converted into fatty acyl-CoAs by acyl-CoA synthetase (encoded by *Acsl*) and then esterified with glycerol to form TGs, with the last step catalyzed by

diglyceride acyltransferase (encoded by *Dgat*) (42). We assayed several key enzymes in adipocyte fatty acid uptake and lipogenesis and observed sex- and depot-specific differences in *Fabp4*, *Fatp4* and *Dgat1* mRNA expression in isolated mature adipocytes. *Fabp4* was 36% lower in the parametrial-periovarian depot of female *Klf14*-deficient mice ($\beta_{\text{Female pWAT}}$=-10.750, $P_{\text{Female pWAT}}=3 \times 10^{-4}$) (Figure 6E) while *Fatp4* (Figure 6F) and *Dgat1* (Figure 6G) was 20% and 54% higher in the parametrial-periovarian depot of the same mice compared to WT controls ($\beta_{\text{Female pWAT}}$=14.336, $P_{\text{Female pWAT}}=8 \times 10^{-5}$). We also observed differences in other pathway genes that were either sex- or depot-specific. mRNA levels for *Fatp1* were decreased in both female subcutaneous WAT and perigonadal/visceral WAT, *Dgat2* was decreased in male subcutaneous WAT and epididymal/visceral WAT. We also observed that Fabp5 was decreased in both female and male subcutaneous WAT and visceral WAT (Supplementary Figure S4). *Acaca*, *Acacb* and *Fasn* showed no differences. (Supplementary Figure S4).

Adipocyte KLF14 overexpression reduces body fat in female mice

Our results showed that KLF14 deficiency resulted in an adverse metabolic phenotype in female mice. We therefore hypothesized that overexpression of *Klf14* may be metabolically beneficial. To address this, we generated a transgenic mouse with *Klf14* overexpression under the regulation of the *Adipoq* promoter (*Adipoq-Klf14*-OE) (see Material and Methods section for a detailed description). This resulted in 1.7-fold induction of KLF14 in adipocytes (Supplementary Figure 1C). We fed these mice a high fat diet for 18 weeks and performed body composition analysis using EchoMRI. Male and female mice from both genotypes gained similar amounts of body weight, and no difference in body weight between the *Klf*14-overexpressing mice (*Adipoq-Klf14*-OE) and WT littermates were observed at the end of the 18-week diet challenge (Figure 7A). However, starting at 12 weeks of HFD, female *Adipoq-Klf14*-OE mice showed a trend towards decreased fat mass to lean mass ratios compared to WT littermates (Figure 7B, P=0.074). At the end of the study, after 18 weeks of high fat diet, female mice with *Klf14* overexpression in adipocytes had 38% lower body fat compared to WT littermates (Figure 7B, β_{Female}=-1.446, P_{Female}= 0.002). No differences were observed in male mice with *Klf14* overexpression (Figure 7C, P=0.99).

In summary (Figure 8), *Klf14* deficiency in adipocytes caused major abnormalities in high fat diet-fed female but not male mice. Female adipocyte *Klf14*-deficient mice had increased total body fat with larger visceral fat mass and bigger visceral adipocytes, but they had smaller subcutaneous adipocytes. Concomitant with the changes in body fat distribution and adipocyte size, the mice demonstrate metabolic abnormalities including insulin resistance and altered serum lipid levels. Despite high fat diet feeding, *Kfl14*-deficient female mice used carbohydrates as the predominant source of energy and simultaneously had lower energy expenditure and activity. Further evaluation of lipid metabolism uncovered defects in fasting- and beta-adrenergic induced lipolysis, and impaired triglyceride and NEFA clearance after lipid gavage. These defects were coupled with decreased mRNA expression of *Pnpla2* (a key lipolytic enzyme) in both perigonadal/visceral and subcutaneous adipocytes. Furthermore, mRNA levels for proteins involved in cellular fatty acid uptake including Fabp4, Fabp5, and Fatp1 were decreased in both subcutaneous WAT and perigonadal/visceral WAT, but mRNA levels of the fatty acid transport protein Fatp4 and Dgat1, an enzyme that catalyzes the conversion of DAG into triglycerides, were increased only in perigonadal/visceral adipocytes. In contrast, adipocyte-*Klf14*-deficient male mice on a HFD gained less body weight, had decreased total body fat with smaller epididymal/visceral and subcutaneous fat depots and adipocytes, but had, relative to wild type, normal metabolic parameters and insulin sensitivity. The male also did not show defects in stimulated lipolysis and lipid clearance, and mRNA levels of enzymes involved in cellular lipid metabolism were not different from wild type littermates, except that Fatp1 was increased in sWAT, and Fabp5 and Dgat2 decreased in subcutaneous WAT and epididymal/visceral WAT. In conclusion, our findings suggest that KLF14 regulates adipose tissue mass and adipocyte size in a depot specific and sex specific manner most likely by differentially modifying adipocyte lipid metabolism.

DISCUSSION

Visceral adipose tissue expansion independent of overall adiposity is associated with an increased risk for developing T2D and cardiovascular disease (43). How deposition of excess calories into the different adipose depots is regulated is currently unknown. However, sex-dependent differences in adipose tissue distribution are well-documented with higher adiposity in females than males (44). Males usually display “android” or “apple shape” distribution with more visceral fat in the abdominal region, while females have “gynoid” or “pear shape” distribution with more subcutaneous fat and less visceral fat in the lower body (45). A shift in fat deposition from subcutaneous depots around the hip to visceral depots in the waist region in males confers increased risk for metabolic disorders (46). However, females can harbor increased upper-body fat without enhanced metabolic disease risk as excess fat is mainly stored in subcutaneous depots. Our results suggest that the transcription factor KLF14 plays a role in modifying adipocyte function and thereby adipose tissue distribution in a sex- and depot-specific manner. Deletion of the *Klf14* gene in mature adipocytes resulted in an increase of visceral fat in female mice but a decrease in male mice. The shift in lipid storage from subcutaneous to parametrial-periovarian (visceral) depots in female mice with adipocyte *Klf14* deletion was characterized by changes in adipocyte size, smaller adipocytes in subcutaneous and larger adipocytes in perigonadal/visceral adipose tissues and major abnormalities in lipid metabolism.

Sex hormones play a significant role in sex-specific body fat distribution, as evidenced by the fact that android and gynoid fat distribution patterns in males and females appear as early as puberty (47). However, circulating levels of testosterone, progesterone and estradiol at 29 weeks of HFD were comparable between female and male adipocyte-*Klf14*-deficient and wild type mice (Supplementary Figure 5), suggesting that the sex differences we observed in mice are likely hormone independent. It is however possible that differential expression of sex hormone receptors or sex-specific interactions of KLF14 with sex hormone receptors could play a role in transcriptional target expression; other KLF family transcription factors cobind DNA with the estrogen receptor. We do not know how KLF14 affects body fat distribution and impacts adipocyte function distinctly in different sexes. KLF14 has been shown to be a master regulator of adipose tissue gene expression

(1). We speculate that differential expression of sex hormone receptors or sex-specific interactions of KLF14 with sex hormone receptors could play a role in transcriptional target expression, especially since, other KLF family transcription factors have been shown to cobind DNA with the estrogen receptor (48). Primary targets in male and female adipocytes need to be established.

The absence of *Klf14* in adipocytes causes significant abnormalities in lipid metabolism, both lipolysis and fatty acid uptake in female mice. Whether these are primary consequences of KLF14 deficiency or secondary metabolic abnormalities due to changes in adipose tissue mass and distribution, and adipocyte size is not entirely clear. Future identification of the primary consequences of KLF14 deficiency on metabolism and primary Klf14 targets will require the careful analysis of metabolic phenotypes at various time points before and after the transition to HF diet. Abnormalities in circulating lipids in female mice with *Klf14*-deficiency in adipocytes can partly be explained by the increased insulin resistance in adipocyte *Klf14*-deficient female mice. This includes the lower circulating HDL-C and increased plasma triglyceride levels under fasting condition, and impaired triglyceride and NEFA clearance after lipid gavage. Triglyceride clearance requires the action of lipoprotein lipase in adipose tissues and insulin-stimulated lipoprotein lipase activity is impaired in insulin resistance. Insulin-stimulated NEFA uptake under fed conditions is also defective in insulin resistance. Furthermore, expression of fatty acid transporters is decreased in the presence of impaired insulin sensitivity (49). However, the lower-than-normal NEFA levels in female mice under fed and fasting conditions and in response to beta-adrenergic stimulation cannot be attributed to impaired insulin sensitivity. On the contrary, NEFA levels should be increased due to defective suppression of lipolysis by insulin. Currently, we do not know the mechanisms by which *Klf14*-deficiency in adipocytes impairs lipolysis. But impaired lipolysis is accompanied by a decrease in *Pnpla2* mRNA in adipocytes of both sWAT and pWAT in female mice. Since KLF14's DNA binding motif is not well-established, future studies will establish if ATGL is a primary target of KLF14.

Hormone sensitive lipase (HSL) was once thought to be the key enzyme that regulates cellular TG breakdown. Its activity is modulated by phosphorylation (33) However, *Hsl* deficient mice had a normal rate of FFA

production, indicating that other enzymes are playing a key role in TG breakdown (50). Haemmerle *et al.* identified ATGL as the rate limiting enzyme in the mobilization of cellular TG (51). Notably, they reported that mice with inactivated ATGL displayed deleterious metabolic phenotypes similar to those of our female adipocyte *Klf14*-deficient mice. These include increased adipose tissue mass, decreased insulin sensitivity, and decreased availability of FFAs (51). The latter fostered the use of carbohydrates as the primary fuel despite the presence of increased amounts of fat in the adipose tissue. Reduced TG hydrolysis then led to reduced energy expenditure and total activity. This study supports the notion that defective lipolysis in adipocyte *Klf14*-deficient mice leads to the switch to carbohydrates as the predominant source of energy, the decrease in energy expenditure and activity, and increased fat mass gain. The fact that glucose tolerance is not impaired in adipocyte *Klf14*-deficient mice despite impaired insulin sensitivity may be explained by the energy substrate switch to glucose and decreased cellular NEFA uptake facilitating instead glucose uptake into tissues.

The increased size of parametrial/visceral adipocytes in females with adipocyte *Klf14*-deficiency can be explained by impaired lipolysis as visceral adipocytes are normally more lipolytic than subcutaneous adipocytes (34). But increased expression of *Dgat1* in parametrial/visceral adipocytes may further contribute to increased adipocyte size. Mice overexpressing Dgat1 in adipocytes have increased deposition of TG in WAT (52). Although fatty acid uptake is impaired in adipocytes, as decreased expression of key fatty acid binding/transporter proteins and impaired NEFA clearance suggest, fatty acids taken up could be efficiently esterified to TG due to the increase in *Dgat1*. Increased *Dgat1* expression cannot be explained by increased insulin resistance. In contrast, Dgat1 expression positively correlates with insulin sensitivity in human subjects (53). Specific transcription factors regulating Dgat1 expression have not been identified, but PPARγ is a candidate (54). Whether KLF14 directly or indirectly controls Dgat1 expression will need to be investigated.

Interestingly, male mice despite decreased fat mass and smaller adipocytes did not show improved metabolic parameters and greater insulin sensitivity when compared to wild type littermates. It is possible that simultaneous changes in fatty acid transporter/binding proteins in the smaller adipocytes are leading to unfavorable changes that are, however, offset by improved insulin sensitivity.

Previous mouse studies showed conflicting results for KLF14 on metabolic phenotypes and atherosclerosis. We recently reviewed these studies (5), several of which only used male mice to study the impact of KLF14 deletion or ectopic overexpression, a consequential omission given that in humans and in our study, KLF14 plays sexual-dimorphic roles. Some of the studies also used different diet compositions which may be the source of the conflicting results.

Finally, we showed a metabolically favorable consequence of increased expression of adipocyte KLF14 since female overexpression mice accumulated less body fat in response to a HF diet challenge. Previous studies showed that perhexiline, an approved therapeutic small molecule presently in clinical use to treat angina and heart failure, induced KLF14 expression and reduced atherosclerosis (55). Our results, together with the results from this previous pharmacological study, suggest that therapeutic targeting of KLF14, specifically in adipose tissue, may lead to an improved metabolic phenotype.

Acknowledgements We thank the members of the Civelek laboratory for their feedback and discussion. We thank Dr. Stephen B. Abbott for the assistance in indirect calorimetry analysis. We thank Dr. Michael M. Scott for the assistance in EchoMRI.

Funding This work was supported by R01 DK118287 from the National Institute of Diabetes and Digestive and Kidney Diseases (to M. Civelek) and 1-19-IBS-105 from the American Diabetes Association (to M. Civelek).

Duality of Interest K. Musunuru is an advisor to and holds equity in Verve Therapeutics and Variant Bio.

Author Contributions Q. Yang and M. Civelek conceived the study; J. Hinkle, J.N. Reed, R. Aherrahrou, Z. Xu participated in data collection and analysis. K. Musunuru generated *Klf14*$^{fl/fl}$*Adipoq*-Cre+ mice. T. E. Harris, E. J. Stephenson, and S.R. Keller contributed to the experimental design and data interpretation. Q. Yang, S.R. Keller and M. Civelek drafted the article. M. Civelek directed the study. All authors edited the final article. M. Civelek is the guarantor of this work and, as such, had full access to all the data in the study and takes responsibility for the integrity of the data and the accuracy of the data analysis.

REFERENCES

1. Small KS, Todorčević M, Civelek M, Moustafa JSE-S, Wang X, Simon MM, et al. Regulatory variants at KLF14 influence type 2 diabetes risk via a female-specific effect on adipocyte size and body composition. Nature Genetics. 2018 Apr;50(4):572.
2. Teslovich TM, Musunuru K, Smith AV, Edmondson AC, Stylianou IM, Koseki M, et al. Biological, clinical and population relevance of 95 loci for blood lipids. Nature. 2010 Aug 5;466(7307):707–13.
3. Voight BF, Scott LJ, Steinthorsdottir V, Morris AP, Dina C, Welch RP, et al. Twelve type 2 diabetes susceptibility loci identified through large-scale association analysis. Nat Genet. 2010 Jul;42(7):579–89.
4. Chen G, Bentley A, Adeyemo A, Shriner D, Zhou J, Doumatey A, et al. Genome-wide association study identifies novel loci association with fasting insulin and insulin resistance in African Americans. Hum Mol Genet. 2012 Oct 15;21(20):4530–6.
5. Yang Q, Civelek M. Transcription Factor KLF14 and Metabolic Syndrome. Front Cardiovasc Med. 2020;7:91.
6. Civelek M, Wu Y, Pan C, Raulerson CK, Ko A, He A, et al. Genetic Regulation of Adipose Gene Expression and Cardio-Metabolic Traits. Am J Hum Genet. 2017 Mar 2;100(3):428–43.
7. Civelek M, Lusis AJ. Systems genetics approaches to understand complex traits. Nat Rev Genet. 2014 Jan;15(1):34–48.
8. Civelek M, Lusis AJ. Conducting the metabolic syndrome orchestra. Nat Genet. 2011 Jun;43(6):506–8.
9. GTEx Consortium. The Genotype-Tissue Expression (GTEx) project. Nat Genet. 2013 Jun;45(6):580–5.
10. Small KS, Hedman AK, Grundberg E, Nica AC, Thorleifsson G, Kong A, et al. Identification of an imprinted master trans regulator at the KLF14 locus related to multiple metabolic phenotypes. Nat Genet. 2011 Jun;43(6):561–4.
11. Liu DJ, Peloso GM, Yu H, Butterworth AS, Wang X, Mahajan A, et al. Exome-wide association study of plasma lipids in >300,000 individuals. Nat Genet. 2017 Dec;49(12):1758–66.
12. Willer CJ, Schmidt EM, Sengupta S, Peloso GM, Gustafsson S, Kanoni S, et al. Discovery and refinement of loci associated with lipid levels. Nat Genet. 2013 Nov;45(11):1274–83.
13. Jones AS, Johnson MS, Nagy TR. Validation of quantitative magnetic resonance for the determination of body composition of mice. Int J Body Compos Res. 2009;7(2):67–72.
14. Fantin VR, Wang Q, Lienhard GE, Keller SR. Mice lacking insulin receptor substrate 4 exhibit mild defects in growth, reproduction, and glucose homeostasis. Am J Physiol Endocrinol Metab. 2000 Jan;278(1):E127-133.
15. Wortley KE, Rincon J-P del, Murray JD, Garcia K, Iida K, Thorner MO, et al. Absence of ghrelin protects against early-onset obesity. J Clin Invest. 2005 Dec 1;115(12):3573–8.
16. Fentz J, Kjøbsted R, Birk JB, Jordy AB, Jeppesen J, Thorsen K, et al. AMPKα is critical for enhancing skeletal muscle fatty acid utilization during in vivo exercise in mice. The FASEB Journal. 2015;29(5):1725–38.
17. Hargett SR, Walker NN, Hussain SS, Hoehn KL, Keller SR. Deletion of the Rab GAP Tbc1d1 modifies glucose, lipid, and energy homeostasis in mice. Am J Physiol Endocrinol Metab. 2015 Aug 1;309(3):E233-245.
18. Berry R, Church CD, Gericke MT, Jeffery E, Colman L, Rodeheffer MS. Imaging of adipose tissue. Methods Enzymol. 2014;537:47–73.
19. Schneider CA, Rasband WS, Eliceiri KW. NIH Image to ImageJ: 25 years of Image Analysis. Nat Methods. 2012 Jul;9(7):671–5.
20. Parlee SD, Lentz SI, Mori H, MacDougald OA. Quantifying size and number of adipocytes in adipose tissue. Methods Enzymol. 2014;537:93–122.
21. Fan W, Xu Y, Liu Y, Zhang Z, Lu L, Ding Z. Obesity or Overweight, a Chronic Inflammatory Status in Male Reproductive System, Leads to Mice and Human Subfertility. Front Physiol. 2018;8.
22. Kumar A, Lawrence JC, Jung DY, Ko HJ, Keller SR, Kim JK, et al. Fat cell-specific ablation of rictor in mice impairs insulin-regulated fat cell and whole-body glucose and lipid metabolism. Diabetes. 2010 Jun;59(6):1397–406.

23. Cirera S. Highly efficient method for isolation of total RNA from adipose tissue. BMC Res Notes. 2013 Nov 18;6:472.
24. Kwon H, Kim D, Kim JS. Body Fat Distribution and the Risk of Incident Metabolic Syndrome: A Longitudinal Cohort Study. Sci Rep. 2017 Sep 8;7(1):10955.
25. Després J-P, Lemieux I, Bergeron J, Pibarot P, Mathieu P, Larose E, et al. Abdominal Obesity and the Metabolic Syndrome: Contribution to Global Cardiometabolic Risk. Arteriosclerosis, Thrombosis, and Vascular Biology. 2008 Jun 1;28(6):1039–49.
26. Björntorp P, Sjöström L. Number and size of adipose tissue fat cells in relation to metabolism in human obesity. Metabolism. 1971 Jul 1;20(7):703–13.
27. Björntorp P, Grimby G, Sanne H, Sjöström L, Tibblin G, Wilhelmsen L. Adipose tissue fat cell size in relation to metabolism in weight-stabile, physically active men. Horm Metab Res. 1972 May;4(3):182–6.
28. Haller H, Leonhardt W, Hanefeld M, Julius U. Relationship between adipocyte hypertrophy and metabolic disturbances. Endokrinologie. 1979 Apr;74(1):63–72.
29. Salans LB, Knittle JL, Hirsch J. The role of adipose cell size and adipose tissue insulin sensitivity in the carbohydrate intolerance of human obesity. J Clin Invest. 1968 Jan;47(1):153–65.
30. Duncan RE, Ahmadian M, Jaworski K, Sarkadi-Nagy E, Sul HS. Regulation of Lipolysis in Adipocytes. Annu Rev Nutr. 2007;27:79–101.
31. Fain JN, Garcĩa-Sáinz JA. Adrenergic regulation of adipocyte metabolism. J Lipid Res. 1983 Aug;24(8):945–66.
32. Morimoto C, Tsujita T, Sumida M, Okuda H. Substrate-Dependent Lipolysis Induced by Isoproterenol. Biochemical and Biophysical Research Communications. 2000 Aug 11;274(3):631–4.
33. Watt MJ, Holmes AG, Pinnamaneni SK, Garnham AP, Steinberg GR, Kemp BE, et al. Regulation of HSL serine phosphorylation in skeletal muscle and adipose tissue. American Journal of Physiology-Endocrinology and Metabolism. 2006 Mar 1;290(3):E500–8.
34. Ibrahim MM. Subcutaneous and visceral adipose tissue: structural and functional differences. Obesity Reviews. 2010;11(1):11–8.
35. Abumrad N, Harmon C, Ibrahimi A. Membrane transport of long-chain fatty acids: evidence for a facilitated process. J Lipid Res. 1998 Dec;39(12):2309–18.
36. Febbraio M, Hajjar DP, Silverstein RL. CD36: a class B scavenger receptor involved in angiogenesis, atherosclerosis, inflammation, and lipid metabolism. J Clin Invest. 2001 Sep;108(6):785–91.
37. Abumrad NA, el-Maghrabi MR, Amri EZ, Lopez E, Grimaldi PA. Cloning of a rat adipocyte membrane protein implicated in binding or transport of long-chain fatty acids that is induced during preadipocyte differentiation. Homology with human CD36. J Biol Chem. 1993 Aug 25;268(24):17665–8.
38. Haq RU, Christodoulides L, Ketterer B, Shrago E. Characterization and purification of fatty acid-binding protein in rat and human adipose tissue. Biochim Biophys Acta. 1982 Nov 12;713(2):193–8.
39. Linn TC, Srere PA. Identification of ATP citrate lyase as a phosphoprotein. J Biol Chem. 1979 Mar 10;254(5):1691–8.
40. Wakil SJ. A malonic acid derivative as an intermediate in fatty acid synthesis. J Am Chem Soc. 1958 Dec 1;80(23):6465–6465.
41. Alberts AW, Strauss AW, Hennessy S, Vagelos PR. Regulation of synthesis of hepatic fatty acid synthetase: binding of fatty acid synthetase antibodies to polysomes. Proc Natl Acad Sci U S A. 1975 Oct;72(10):3956–60.
42. Cases S, Smith SJ, Zheng YW, Myers HM, Lear SR, Sande E, et al. Identification of a gene encoding an acyl CoA:diacylglycerol acyltransferase, a key enzyme in triacylglycerol synthesis. Proc Natl Acad Sci U S A. 1998 Oct 27;95(22):13018–23.
43. Bjørndal B, Burri L, Staalesen V, Skorve J, Berge RK. Different adipose depots: their role in the development of metabolic syndrome and mitochondrial response to hypolipidemic agents. J Obes. 2011;2011:490650.
44. Gallagher D, Visser M, Sepúlveda D, Pierson RN, Harris T, Heymsfield SB. How useful is body mass index for comparison of body fatness across age, sex, and ethnic groups? Am J Epidemiol. 1996 Feb 1;143(3):228–39.
45. Schreiner PJ, Terry JG, Evans GW, Hinson WH, Crouse JR, Heiss G. Sex-specific associations of

magnetic resonance imaging-derived intra-abdominal and subcutaneous fat areas with conventional anthropometric indices. The Atherosclerosis Risk in Communities Study. Am J Epidemiol. 1996 Aug 15;144(4):335–45.

46. Demerath EW, Sun SS, Rogers N, Lee M, Reed D, Choh AC, et al. Anatomical patterning of visceral adipose tissue: race, sex, and age variation. Obesity (Silver Spring). 2007 Dec;15(12):2984–93.
47. de Ridder CM, Bruning PF, Zonderland ML, Thijssen JH, Bonfrer JM, Blankenstein MA, et al. Body fat mass, body fat distribution, and plasma hormones in early puberty in females. J Clin Endocrinol Metab. 1990 Apr;70(4):888–93.
48. Simmen RCM, Pabona JMP, Velarde MC, Simmons C, Rahal O, Simmen FA. The emerging role of Krüppel-like factors in endocrine-responsive cancers of female reproductive tissues. J Endocrinol. 2010 Mar;204(3):223–31.
49. Chabowski A, Coort SLM, Calles-Escandon J, Tandon NN, Glatz JFC, Luiken JJFP, et al. Insulin stimulates fatty acid transport by regulating expression of FAT/CD36 but not FABPpm. American Journal of Physiology-Endocrinology and Metabolism. 2004 Oct 1;287(4):E781–9.
50. Osuga J, Ishibashi S, Oka T, Yagyu H, Tozawa R, Fujimoto A, et al. Targeted disruption of hormone-sensitive lipase results in male sterility and adipocyte hypertrophy, but not in obesity. PNAS. 2000 Jan 18;97(2):787–92.
51. Haemmerle G, Lass A, Zimmermann R, Gorkiewicz G, Meyer C, Rozman J, et al. Defective Lipolysis and Altered Energy Metabolism in Mice Lacking Adipose Triglyceride Lipase. Science. 2006 May 5;312(5774):734–7.
52. Chen HC, Stone SJ, Zhou P, Buhman KK, Farese RV. Dissociation of Obesity and Impaired Glucose Disposal in Mice Overexpressing Acyl Coenzyme A:Diacylglycerol Acyltransferase 1 in White Adipose Tissue. Diabetes. 2002 Nov 1;51(11):3189–95.
53. Ranganathan G, Unal R, Pokrovskaya I, Yao-Borengasser A, Phanavanh B, Lecka-Czernik B, et al. The lipogenic enzymes DGAT1, FAS, and LPL in adipose tissue: effects of obesity, insulin resistance, and TZD treatment. Journal of Lipid Research. 2006 Nov 1;47(11):2444–50.
54. Yen C-LE, Stone SJ, Koliwad S, Harris C, Farese RV. Thematic Review Series: Glycerolipids. DGAT enzymes and triacylglycerol biosynthesis. Journal of Lipid Research. 2008 Nov 1;49(11):2283–301.
55. Guo Y, Fan Y, Zhang J, Lomberk GA, Zhou Z, Sun L, et al. Perhexiline activates KLF14 and reduces atherosclerosis by modulating ApoA-I production. J Clin Invest. 2015 Oct 1;125(10):3819–30.

Figure 1:

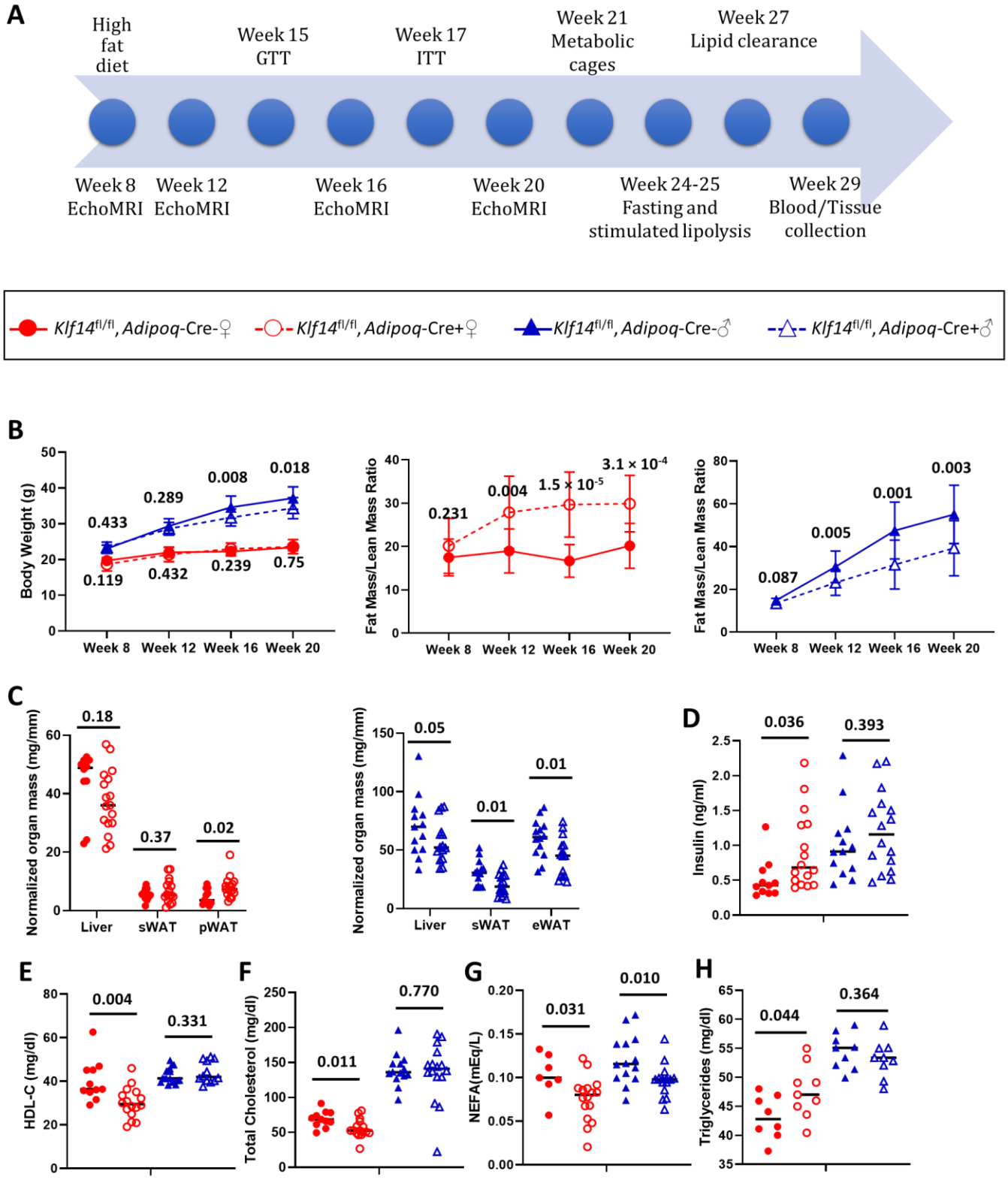

Figure 2:

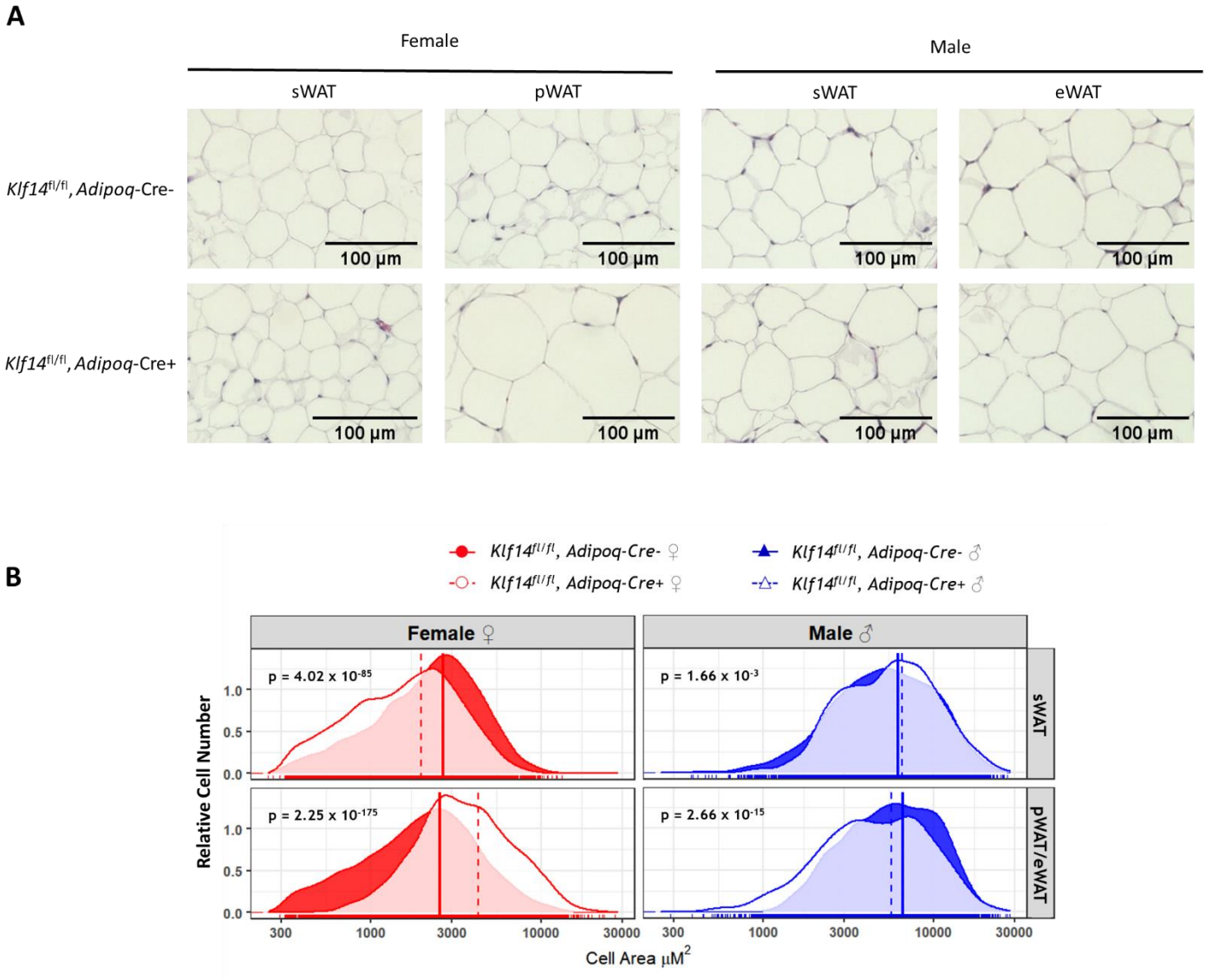

Figure 3:

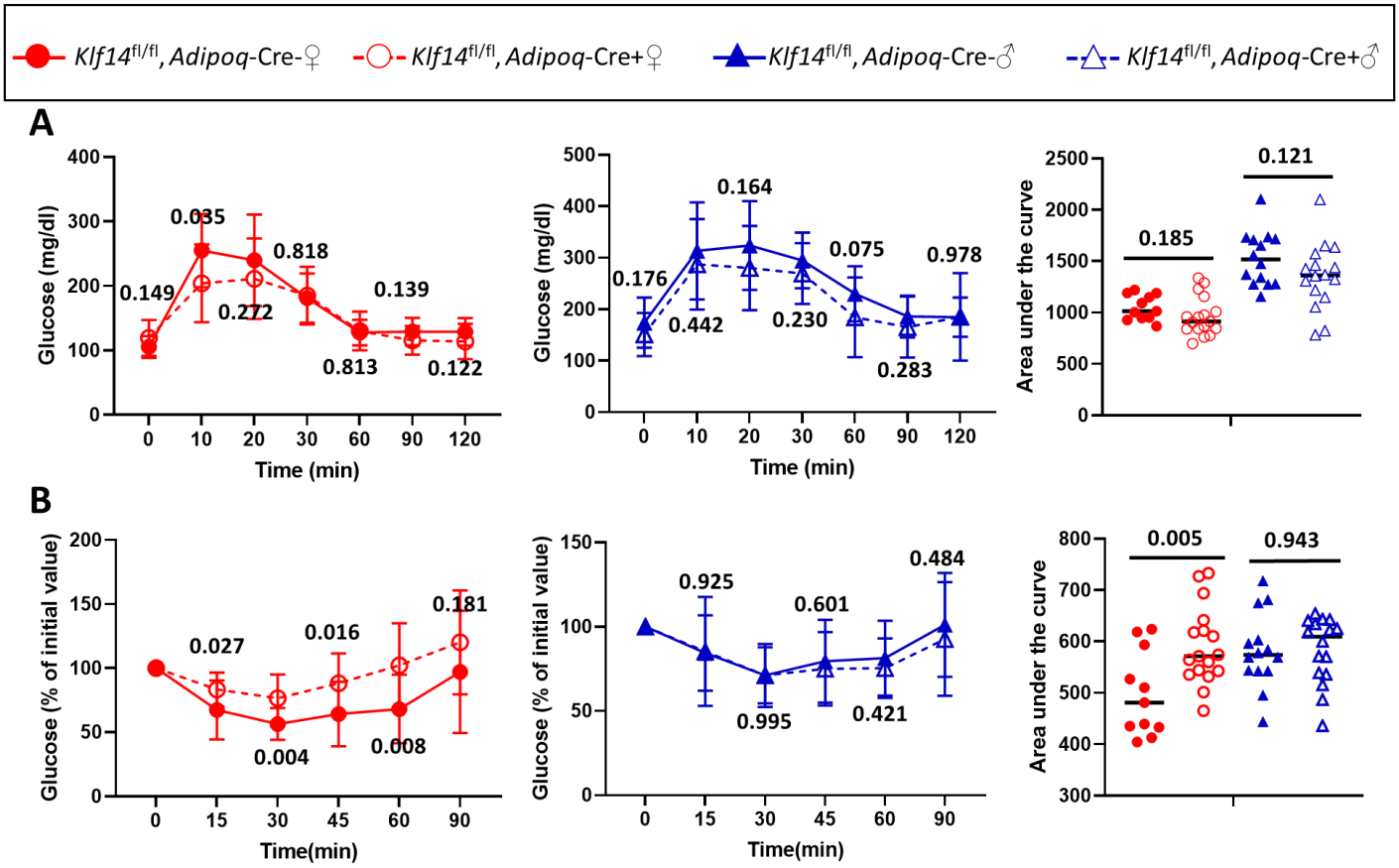

Figure 4:

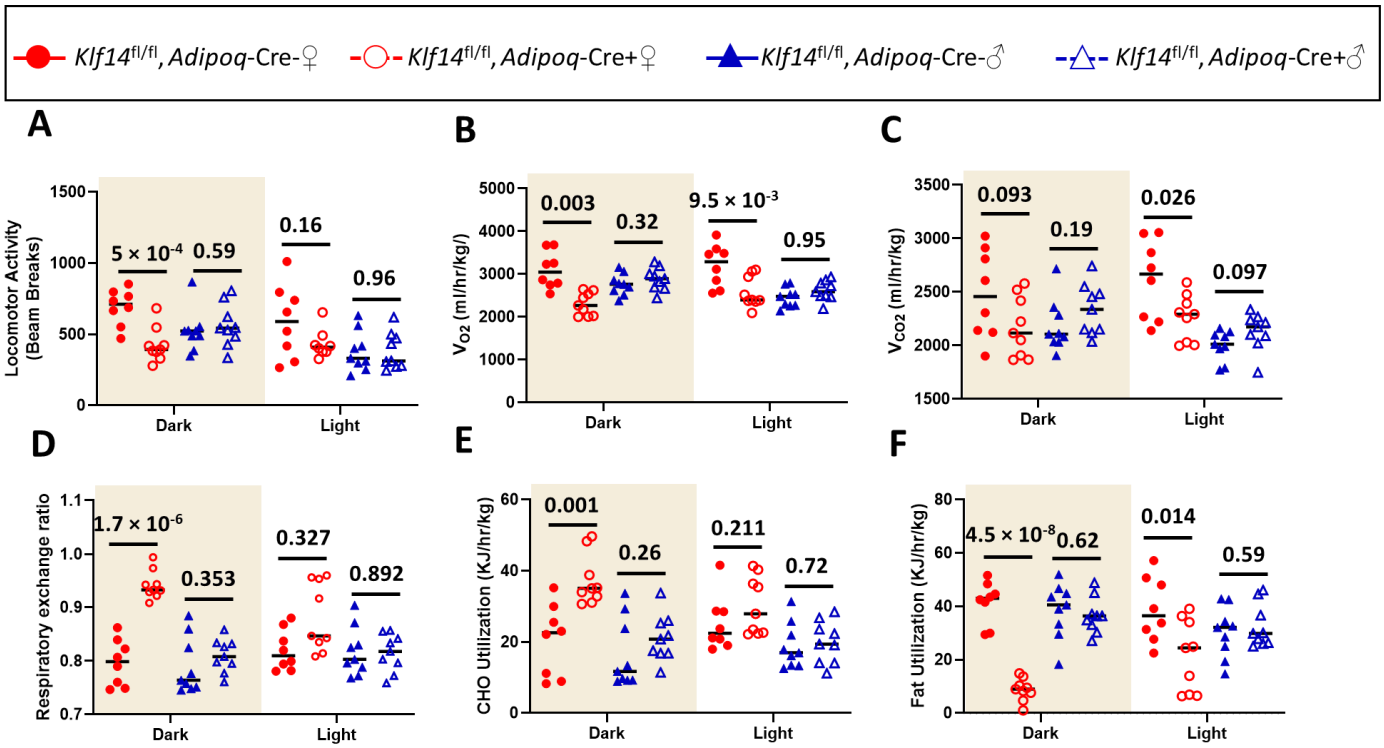

Figure 5:

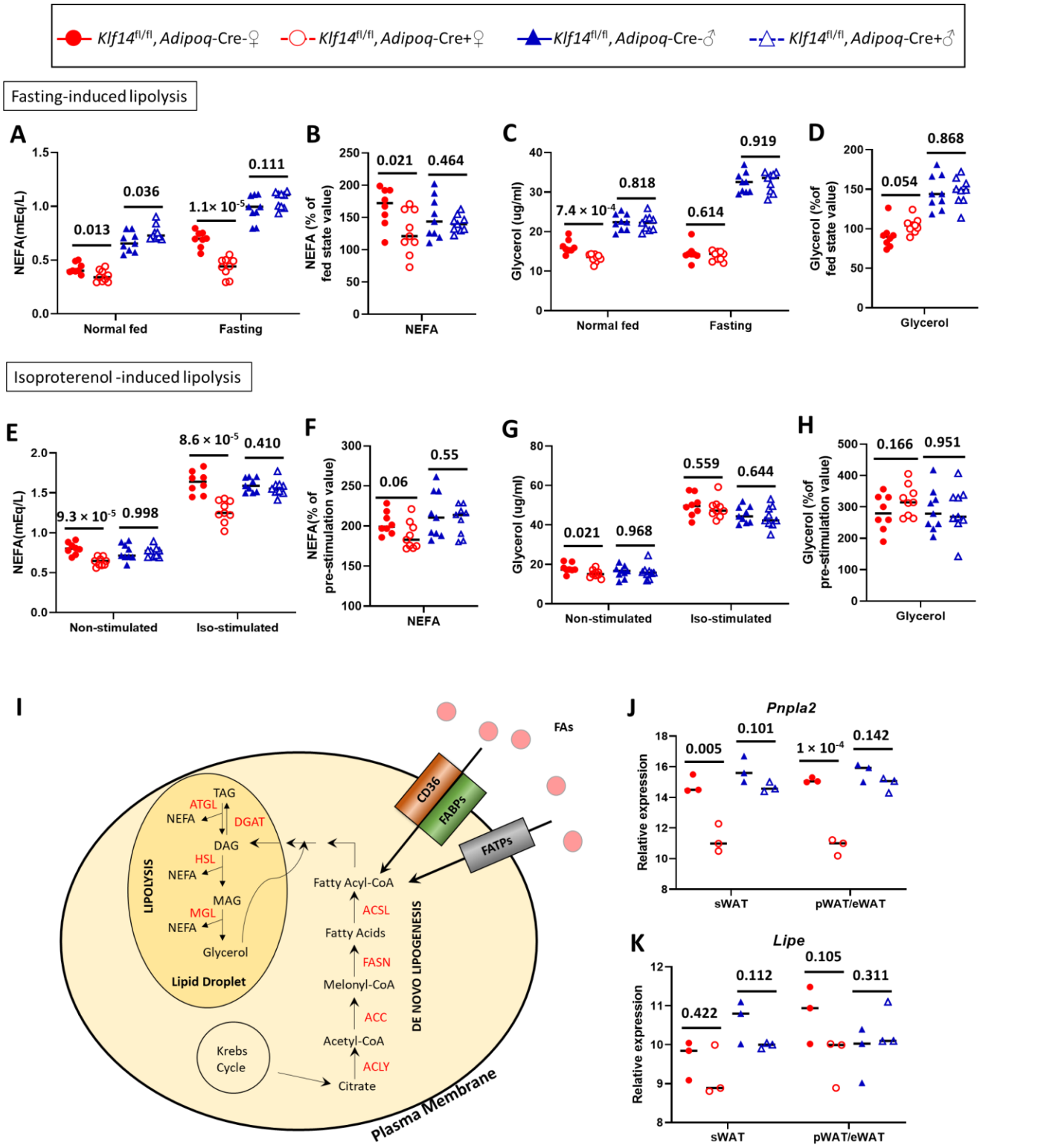

Figure 6:

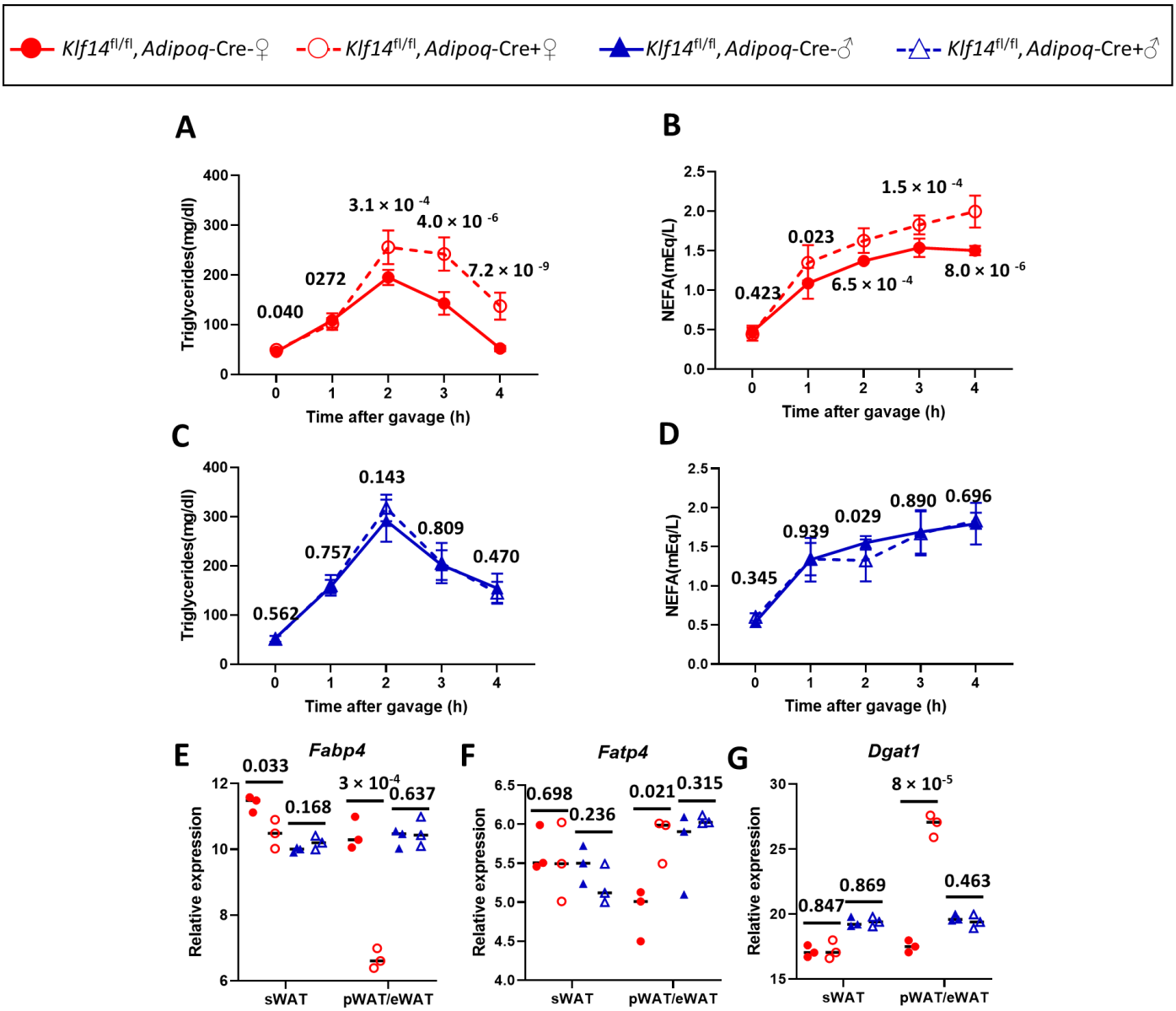

Figure 7:

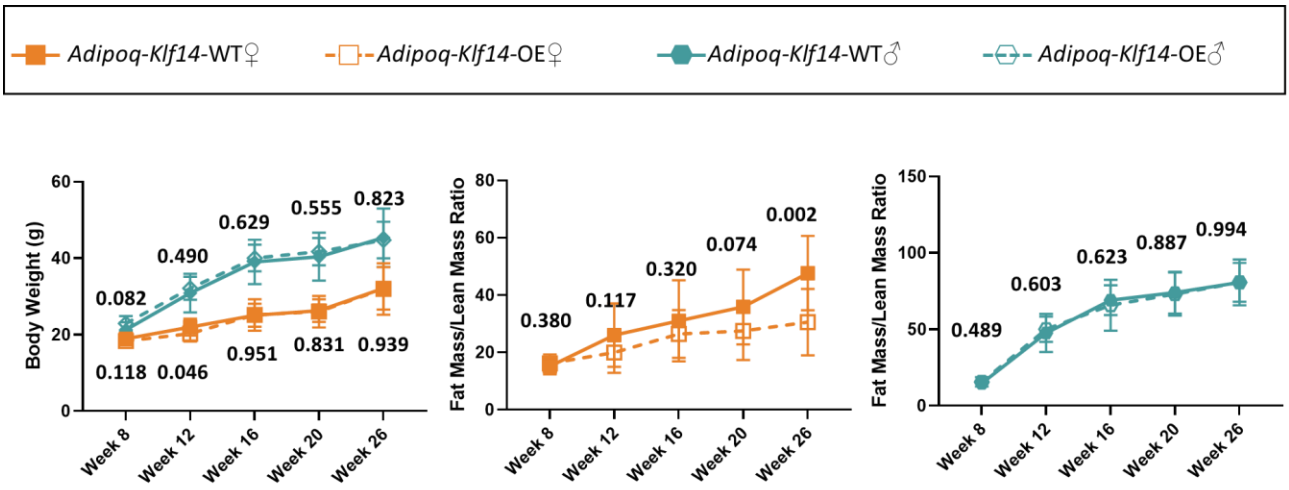

Figure 8:

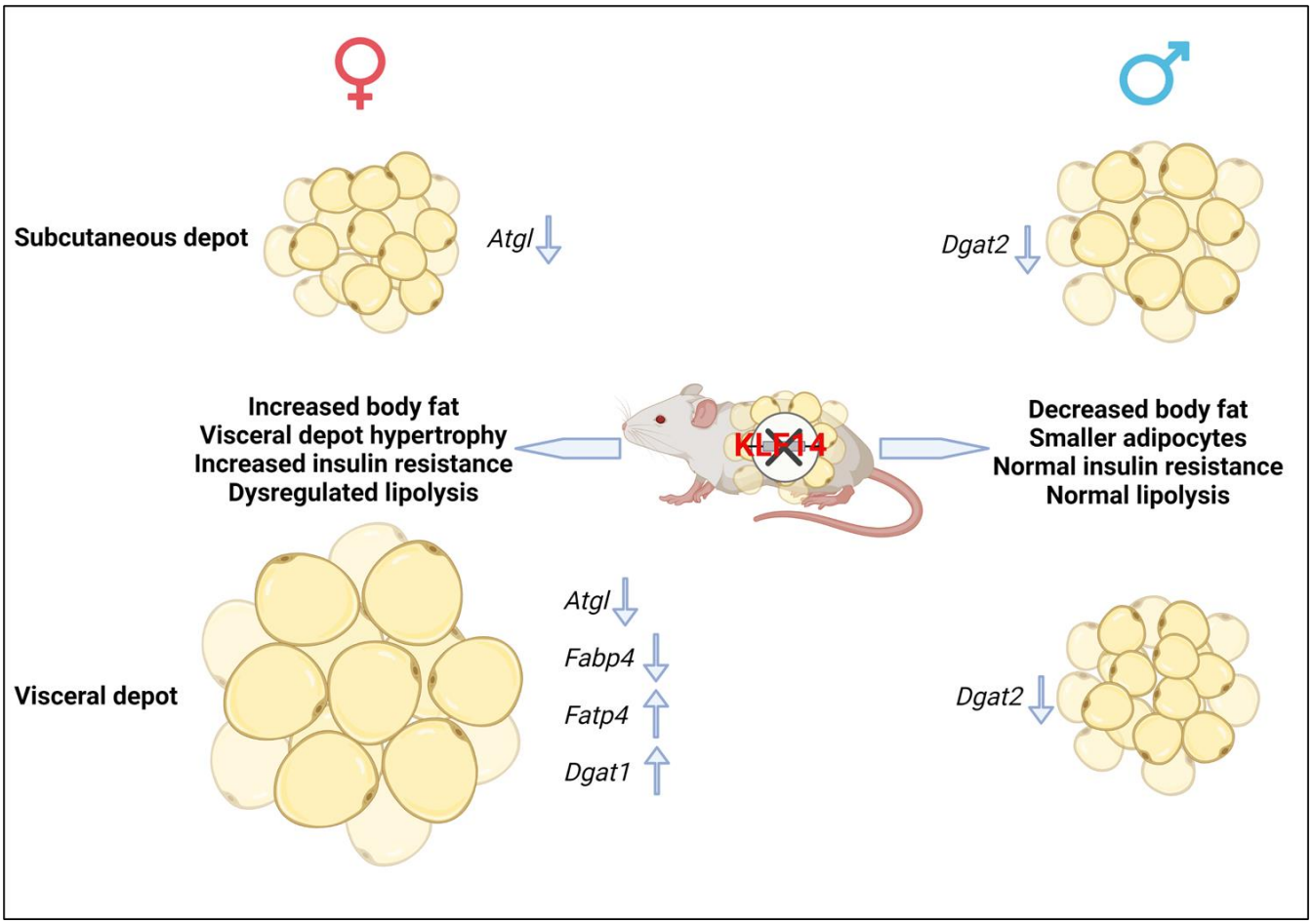

FIGURE LEGENDS

Figure 1. Adipocyte-specific deletion of KLF14 increases fat mass and affects circulating insulin and lipid levels in female mice. (**A)** Experimental design for the metabolic characterization of mice. (**B)** Body weight (left), fat mass/lean mass ratios in female (red) (middle, $N_{Adipoq\text{-}Cre-}$ =11, $N_{Adipoq\text{-}Cre+}$ =17) and male (blue) (right, $N_{Adipoq\text{-}Cre-}$ =14, $N_{Adipoq\text{-}Cre+}$ =14) mice at 8, 12, 16 and 20 weeks of age. (**C)** Normalized organ weights in females (left, $N_{Adipoq\text{-}Cre-}$ =11, $N_{Adipoq\text{-}Cre+}$ =17) and male mice (right, $N_{Adipoq\text{-}Cre-}$ =14, $N_{Adipoq\text{-}Cre+}$=14). sWAT denotes subcutaneous white adipose tissue; pWAT denotes parametrial-periovarian white adipose tissue; and eWAT denotes epididymal white adipose tissue. Plasma/serum levels of (**D)** insulin, (**E)** high-density lipoprotein C (HDL-C), **(F)** total cholesterol, **(G)** non-esterified free fatty acids (NEFA), and **(H)** triglycerides in female ($N_{Adipoq\text{-}Cre-}$ =8-11, $N_{Adipoq\text{-}Cre+}$ =9-17) and male ($N_{Adipoq\text{-}Cre-}$ =9-14, $N_{Adipoq\text{-}Cre+}$ =9-14) at 29 weeks of age after 6 hours of fasting. Data shown **(B)** are mean ∓ standard error of the mean and in **(C-H)** are mean and data for individual mice. *P*-values were calculated using two-tailed unpaired Student's t -tests at each time point for (B) and all data in (C-H).

Figure 2. Adipocyte-specific deletion of KLF14 affects adipocyte size in female mice. (**A)** Representative subcutaneous (sWAT) and visceral (pWAT/eWAT) adipose tissue sections stained with Hematoxylin & Eosin. (**B)** Adipocyte size distribution in subcutaneous (sWAT) and visceral fat depots (pWAT/eWAT) {Citation}of female (red) and male (blue) mice. 5 µm-thick tissue sections from four mice for each genotype and sex were used for the analysis. The number of cells analyzed were as following: $N_{Female\_Adipoq\text{-}Cre\text{-}\_sWAT}$ =3,988; $N_{Female\_Adipoq\text{-}Cre+\_sWAT}$ =5,193; $N_{Female\_Adipoq\text{-}Cre\text{-}\_pWAT}$ =4,132; $N_{Female\_Adipoq\text{-}Cre+\_pWAT}$ =3,218; $N_{Male\_Adipoq\text{-}Cre\text{-}\_sWAT}$ =2,699; $N_{Male\_Adipoq\text{-}Cre+\_sWAT}$ =2,191; $N_{Male\_Adipoq\text{-}Cre\text{-}\_eWAT}$ =2,196; $N_{Male\_Adipoq\text{-}Cre+\_eWAT}$ =2,435 cells. *P*-values were calculated using two-tailed unpaired Student's t -tests.

Figure 3. Adipocyte-specific deletion of KLF14 leads to increased insulin resistance in female mice. Blood glucose concentrations during intraperitoneal **(A)** glucose tolerance tests after 7 weeks of high fat diet and **(B)** insulin tolerance tests after 9 weeks of high fat diet in female (red; left) and male mice (blue; middle). Graphs for area under the curve (AUC) blood glucose concentrations are shown (right). $N_{Female\_Adipoq\text{-}Cre-}$ =11,

$N_{Female\_\textit{Adipoq}\text{-}Cre+}$ =17, $N_{Male\_\textit{Adipoq}\text{-}Cre-}$ =14, $N_{Male\_\textit{Adipoq}\text{-}Cre+}$ =14. Data are mean ∓ standard error of mean. *P*-values were calculated using two-tailed unpaired Student's t -tests at each time point.

Figure 4: Adipocyte-specific deletion of KLF14 modifies energy metabolism in female mice. Indirect calorimetry studies measuring **(A)** total activity, **(B)** oxygen consumption (VO2), **(C)** carbon dioxide production (VCO_2), **(D)** respiratory exchange ratio, **(E)** carbohydrate (CHO) utilization, and **(F)** fat utilization in female (red) and male (blue) mice during dark (shaded area) and light cycles. $N_{Female\_\textit{Adipoq}\text{-}Cre-}$ =8, $N_{Female\_\textit{Adipoq}\text{-}Cre+}$ =9, $N_{Male\_\textit{Adipoq}\text{-}Cre-}$ =9, $N_{Male\_\textit{Adipoq}\text{-}Cre+}$ =9. Mean and individual mouse data are shown. *P*-values were calculated using two-tailed unpaired Student's t -tests.

Figure 5: Adipocyte-specific deletion of KLF14 causes defects in lipolysis in female mice. Mice after a 16-week high-fat diet were fasted for 16 hours. **(A and B)** Fasting non-esterified free fatty acids (NEFA) and **(C and D)** glycerol were measured and compared to that of mice before fasting. Mice after a 17-week high fat diet were treated with 10 mg/kg isoproterenol. Plasma **(E and F)** NEFA and **(G and H)** glycerol was measured and compared to that of mice before stimulation. $N_{Female\_\textit{Adipoq}\text{-}Cre-}$ =8, $N_{Female\_\textit{Adipoq}\text{-}Cre+}$ =9, $N_{Male\_\textit{Adipoq}\text{-}Cre-}$ =9, $N_{Male\_\textit{Adipoq}\text{-}Cre+}$ =9. Changes in plasma levels of NEFA, and glycerol were calculated relative to baseline values (fed-state for B and D or before stimulation for F and H). Mean and individual mouse data are shown. *P*-values were calculated using two-tailed unpaired Student's t-tests. Data from female mice are shown in red and male mice are shown in blue. **(I)** Schematic representation of genes playing a role in triglyceride breakdown (lipolysis) and formation (lipogenesis), and fatty acid uptake. Lipolysis is catalyzed by three lipases: adipose triglyceride lipase (ATGL), hormone-sensitive lipase (HSL), and monoacylglycerol lipase (MGL) whose actions result in the release of NEFA and glycerol. Triglyceride synthesis through de novo lipogenesis uses citrate to make acetyl-CoA by ATP-citrate lyase (ACL), acetyl-CoA is converted to malonyl-CoA by acetyl-CoA carboxylase (ACC), and fatty acid synthesis is achieved by conversion of malonyl-CoA into fatty acids by fatty acid synthase (FASN). Fatty acids are then made into fatty acyl-CoAs by acyl-CoA synthetase (ACSL) and converted to diacylglycerols (DAG) through several enzymatic reactions. Diacylglycerol acyltransferase (DGAT) then catalyzes the conversion of DAG into TAG (triacylglycerol or triglyceride). Cellular uptake of

fatty acids (FAs) is facilitated by CD36, FABPs and FATPs. mRNA expression of **(J)** *Pnpla2* and **(K)** *Lipe* in mature adipocytes isolated from subcutaneous (sWAT) and parametrial-periovarian/epididymal WAT (pWAT/eWAT). N =3 mice per genotype and sex. Relative gene expression, normalized to GAPDH levels, was calculated using the $2^{-\Delta\Delta CT}$ method. *P*-values were calculated using two-tailed unpaired Student's t -tests.

Figure 6: Adipocyte-specific deletion of KLF14 decreases lipid clearance in female mice. Mice on a 19-week high-fat diet were gavaged with a bolus of olive oil. Plasma triglycerides in **(A)** female and **(C)** male mice and non-esterified free fatty acids (NEFA) in **(B)** female and **(D)** male mice were measured over four hours. $N_{Female\_Adipoq\text{-}Cre-}$ =8, $N_{Female\_Adipoq\text{-}Cre+}$ =9, $N_{Male\_Adipoq\text{-}Cre-}$ =9, $N_{Male\_Adipoq\text{-}Cre+}$ =9. mRNA expression of fatty acid uptake gene **(E)** *Fabp4* **(F)** *Fatp4* and de novo lipogenesis gene **(G)** *Dgat1* were measured in mature adipocytes isolated from subcutaneous (sWAT) and parametrial-periovarian/epididymal WAT (pWAT/eWAT). N =3 mice per genotype and sex. Relative gene expression, normalized to GAPDH levels, was calculated using the $2^{-\Delta\Delta CT}$ method. Mean and standard error of the mean are shown in A, B, C, D; mean and individual mouse data are shown in E, F and G. *P*-values were calculated using two-tailed unpaired Student's t -tests. Data from female mice are shown in red and data for male mice are shown in blue.

Figure 7: Adipocyte-specific overexpression of KLF14 decreases fat mass in female mice. Body weight (left), fat mass/lean mass ratio in female (orange) (middle, N_{WT} =14, $N_{Adipoq\text{-}OE}$ =14) and male (blue) (right, N_{WT} =8, $N_{Adipoq\text{-}OE}$ =12) mice at 8, 12, 16, 20, and 26 weeks of age. Data shown are mean ∓ standard error of the mean. *P*-values were calculated using two-tailed unpaired Student's t -test at each time point.

Figure 8: Summary of main findings. Deletion of KLF14 in mouse adipocytes resulted in sex-dimorphic and depot-specific differences. Female mice with adipocyte *Klf14*-deficiency had higher total body fat, primarily due to increased visceral depot fat mass. Female mutant mice also displayed a shift in body fat storage from subcutaneous depot to visceral depot as evidenced by visceral adipocyte hypertrophy and decreased adipocyte size in subcutaneous depots. Meanwhile, male mice had lower body fat mass and smaller cell size in the visceral depots. Female *Klf1*4 knockout mice were insulin resistant while insulin sensitivity in male mice with adipocyte *Klf14*-deficiency was not different from wildtype littermates. Changes in adipose tissue mass and adipocyte size

can, at least in part, be explained by dysregulation of lipid metabolism, including lipolysis, fatty acid uptake and lipogenesis. Several genes involved in these pathways are dysregulated in a sex- and depot-specific manner as indicated.

Adipocyte-specific modulation of KLF14 expression in mice leads to sex-dependent impacts in adiposity and lipid metabolism

Running title: KLF14 is sex-dimorphic in mice metabolism

Qianyi Yang[1], Jameson Hinkle[1], Jordan N. Reed[1,2], Redouane Aherrahrou[1], Zhiwen Xu[3], Thurl E. Harris[4], Erin J. Stephenson[5], Kiran Musunuru[6,7,8], Susanna R. Keller[9], Mete Civelek[1,2]

[1]Center for Public Health Genomics, School of Medicine, University of Virginia, Charlottesville, VA 22908, USA.

[2]Department of Biomedical Engineering, School of Engineering and Applied Science, University of Virginia, Charlottesville, VA 22908, USA.

[3]Department of Chemistry, College of Arts and Sciences, University of Virginia, Charlottesville, VA 22908, USA.

[4]Department of Pharmacology, School of Medicine, University of Virginia, Charlottesville, VA 22908, USA.

[5]Department of Anatomy, College of Graduate Studies & Chicago College of Osteopathic Medicine, Midwestern University, Downers Grove, IL 60515, USA.

[6]Cardiovascular Institute, Perelman School of Medicine at the University of Pennsylvania, Philadelphia, PA, 19104, USA.

[7]Division of Cardiovascular Medicine, Department of Medicine, Perelman School of Medicine at the University of Pennsylvania, Philadelphia, PA, 19104, USA.

[8]Department of Genetics, Perelman School of Medicine at the University of Pennsylvania, Philadelphia, PA, 19104, USA.

[9]Division of Endocrinology and Metabolism, Department of Medicine, School of Medicine, University of Virginia, Charlottesville, VA, 22908, USA.

Corresponding authors:

Qianyi Yang, Ph.D. and Mete Civelek, PhD

University of Virginia

Center for Public Health Genomics

Old Med School 3836

PO Box 800717

Charlottesville, VA 22908-0717

Office Number: 434-243-1669

Fax Number: 434-982-1815

E-mail: qy5sy@virginia.edu and mete@virginia.edu

Word count: 6483

Number of tables: 2 (supplemental)

Number of figures: 8 main figures and 5 supplemental figures

SUPPLEMENTAL FIGURES:

Supplemental Figure 1

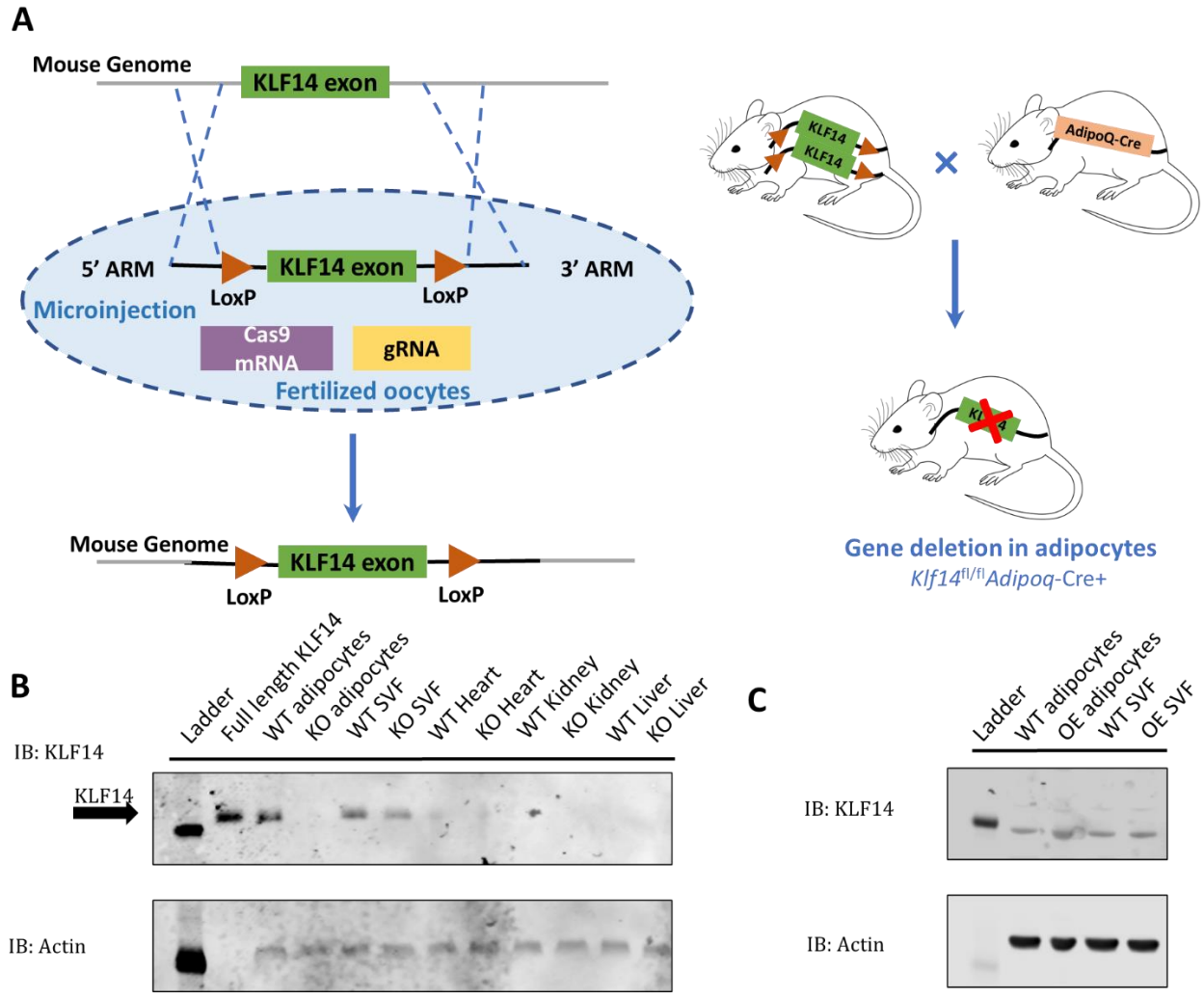

Supplemental Figure 2

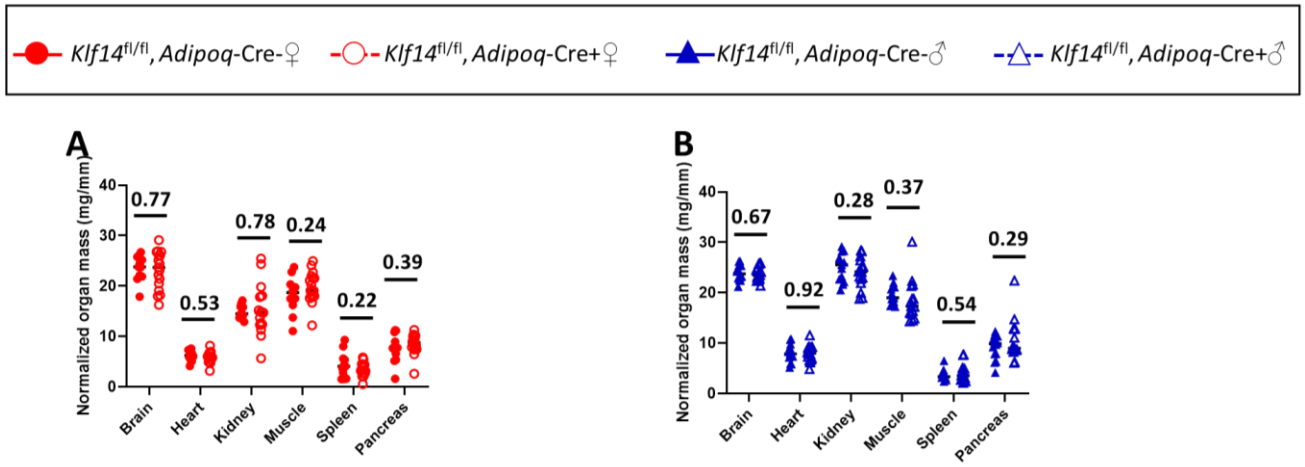

Supplemental Figure 3

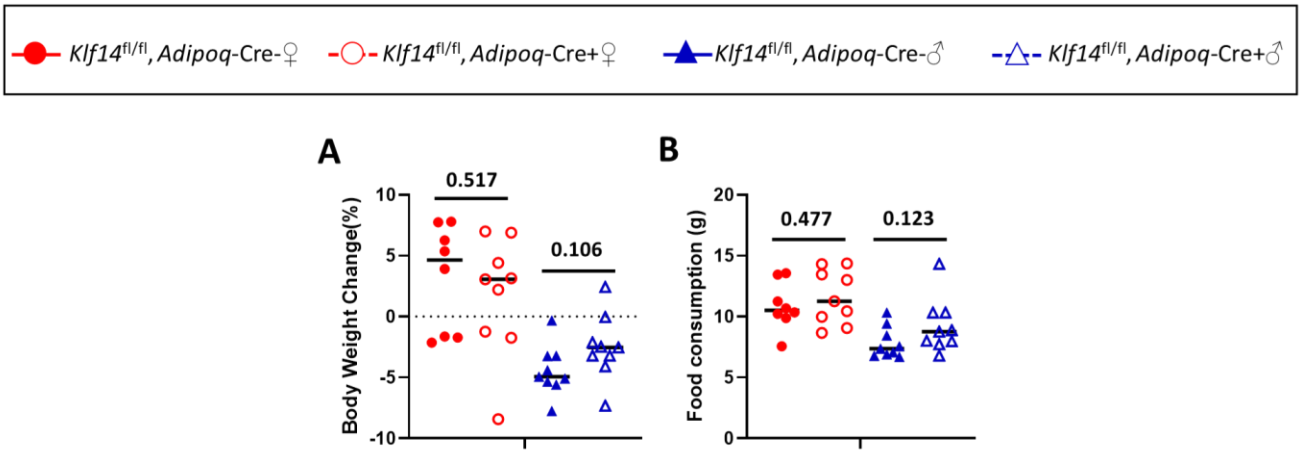

Supplemental Figure 4

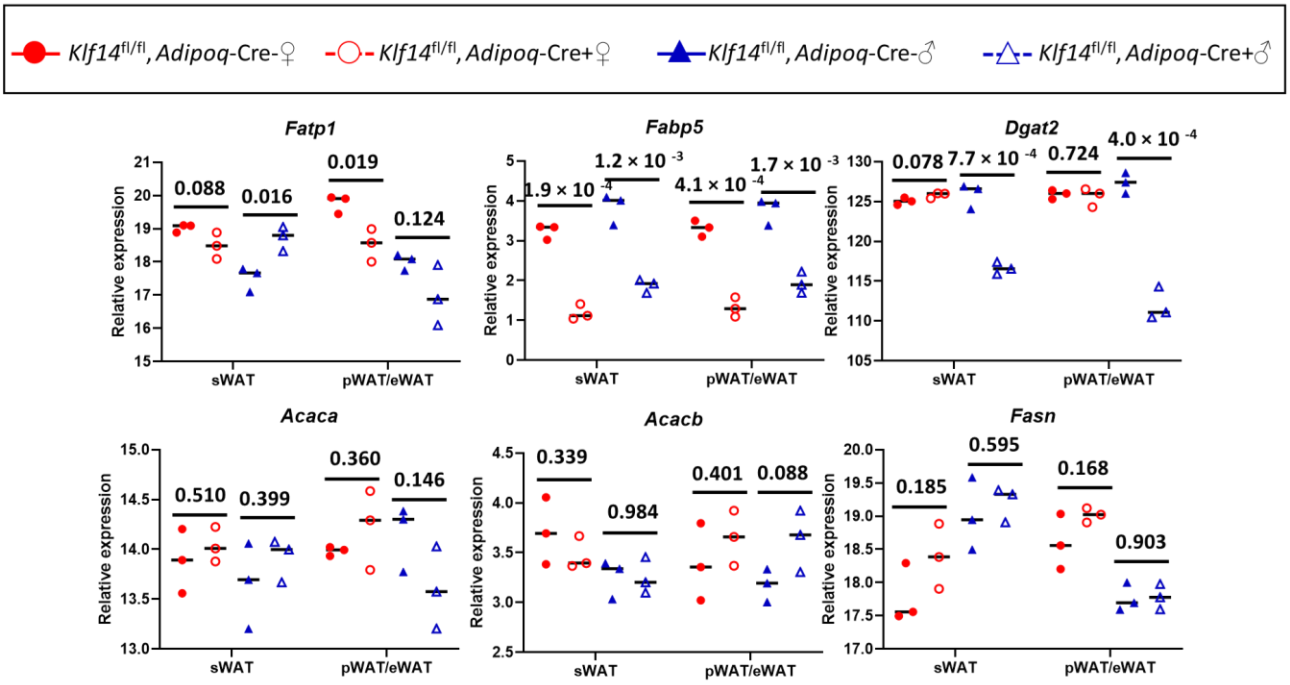

Supplemental Figure 5

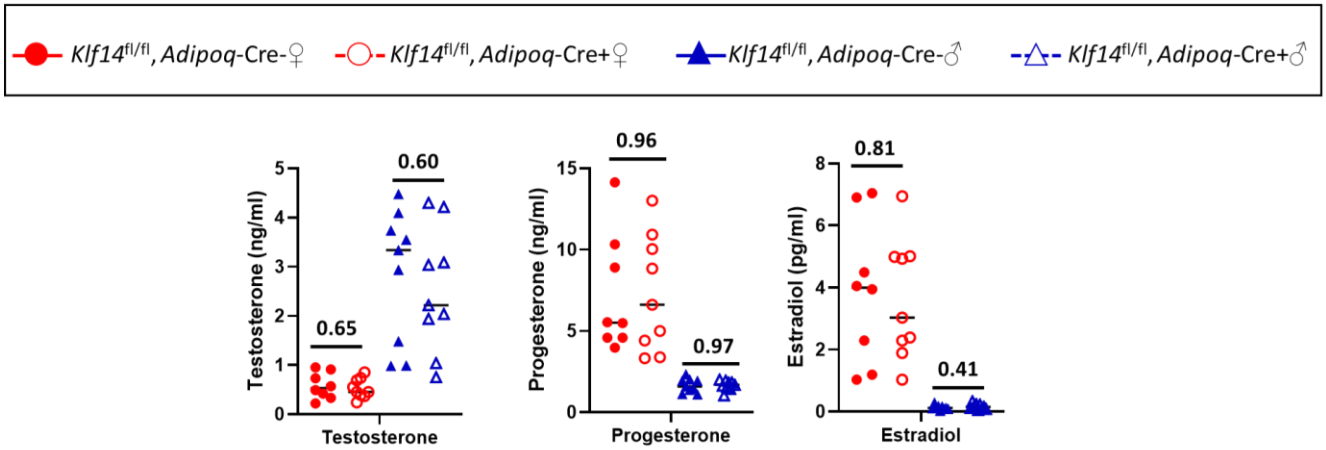

SUPPLEMENTAL FIGURE LEGENDS

Supplemental Figure 1: Characterization of transgenic mice. **(A)** Targeting strategy for deletion of Klf14 in mouse adipocytes. **(B)** KLF14 protein level in adipocytes, stromal vascular fraction (SVF), heart, kidney and liver of wild-type (WT) and knockout (KO) mice. **(C)** KLF14 protein level in adipocytes, stromal vascular fraction (SVF) of wild-type (WT) and overexpression (OE) mice.

Supplemental Figure 2: Tissue weights normalized to tibia length in adipocyte-specific *Klf14* knockout and wild type **(A)** female and **(B)** male mice. $N_{Female,\ Adipoq\text{-}Cre-} = 11$, $N_{Female,Adipoq\text{-}Cre+} = 17$, $N_{Male,Adipoq\text{-}Cre-} = 14$, $N_{Male,Adipoq\text{-}Cre+} = 14$.

Supplemental Figure 3: (A) Body weight change and **(B)** food consumption during the three-day period in metabolic cages. $N_{Female\_Adipoq\text{-}Cre-} = 8$, $N_{Female\_Adipoq\text{-}Cre+} = 9$, $N_{Male\_Adipoq\text{-}Cre-} = 9$, $N_{Male\_Adipoq\text{-}Cre+} = 9$.

Supplemental Figure 4: mRNA expression of fatty acid uptake and metabolism genes *Fatp1, Fabp5, Dgat2, Acaca*, *Acacb*, *Fasn* and in isolated mature adipocytes. N =3 mice per genotype and sex. Relative gene expression, normalized to GAPDH levels, was calculated using the $2^{-\Delta\Delta CT}$ method. *P*-values were calculated using two-tailed unpaired Student's t -test.

Supplemental Figure 5: Sex hormone levels in serum of adipocyte *Klf14*-deficient female and male mice and control littermates at euthanasia after 21 weeks of HFD. (A) Testosterone, (B) Progesterone, (C) Estradiol. $N_{Female\_Adipoq\text{-}Cre-} = 8$, $N_{Female\_Adipoq\text{-}Cre+} = 9$, $N_{Male\_Adipoq\text{-}Cre-} = 9$, $N_{Male\_Adipoq\text{-}Cre+} = 9$.

Supplemental table 1: Mouse genotyping primer list.

Name	Forward	Reverse	Amplicon
Adipoq_Klf14_Cre	GAACCTGATGGACATGTTCAGG	AGTGCGTTCGAACGCTAGAGCCTGT	250bp
Adipoq_Klf14_OE	GGCCTACTACAAGTCGTCGC	CCGGGCTGCAGGAATTCGAT	489bp

Supplemental table 2: qPCR primer list.

Gene	Forward	Reverse	Accession ID	Reference
Fatp1	GGCTCCTGGAGCAGGAACA	ACGGAAGTCCCAGAAACCAA	NM_011977.4	(1)
Fatp4	ACGATGTTTCCTGCTGAGTGGTA	CTCTCCGACCTGCCACAGA	NM_011989.5	(1)
Fabp4	ATGTGCGACCAGTTTGTG	TTTGCCATCCCACTTCTG	NM_024406.3	(2)
Fabp5	GCTGATGGCAGAAAAACTCAGA	CCTGATGCTGAACCAATGCA	NM_001272098.1	(3)
Acc1	CCTCCGTCAGCTCAGATACA	TTTACTAGGTGCAAGCCAGACA	NM_133360.2	(4)
Fasn	GCTGCGGAAACTTCAGGAAAT	AGAGACGTGTCACTCCTGGACTT	NM_007988.3	(5)
Acc2	ACAGAGATTT CACCGTTGCGT	CGCAGCGATGCCATTGT	NM_133904	(6)
Dgat1	ACCGCGAGTTCTACAGAGATTGGT	ACAGCTGCATTGCCATAGTTCCCT	NM_010046.3	(7)
Dgat2	TGGGTCCAGAAGAAGTTCCAGAAGTA	ACCTCAGTCTCTGGAAGGCCAAAT	NM_026384.3	(7)
Hsl	GCTGGGCTGTCAAGCACTGT	GTAACTGGGTAGGCTGCCAT	NM_001039507.2	(8)
Atgl	TGTGGCCTCATTCCTCCTAC	TCGTGGATGTTGGTGGAGCT	NM_001163689.1	(8)
Gapdh	CTCCCACTCTTCCACCTTCG	GCCTCTCTTGCTCAGTGTCC	NM_001289726.1	(9)

1. Mishima T, Miner JH, Morizane M, Stahl A, Sadovsky Y. The Expression and Function of Fatty Acid Transport Protein-2 and -4 in the Murine Placenta. PLoS One [Internet]. 2011 Oct 20 [cited 2021 Jun 14];6(10). Available from: https://www.ncbi.nlm.nih.gov/pmc/articles/PMC3197585/

2. Gan L, Liu Z, Cao W, Zhang Z, Sun C. FABP4 reversed the regulation of leptin on mitochondrial fatty acid oxidation in mice adipocytes. Sci Rep [Internet]. 2015 Aug 27 [cited 2021 Jun 14];5(1):13588. Available from: https://www.nature.com/articles/srep13588

3. Senga S, Kawaguchi K, Kobayashi N, Ando A, Fujii H. A novel fatty acid-binding protein 5-estrogen-related receptor α signaling pathway promotes cell growth and energy metabolism in prostate cancer cells. Oncotarget [Internet]. 2018 Aug 3 [cited 2021 Jun 14];9(60):31753–70. Available from: https://www.ncbi.nlm.nih.gov/pmc/articles/PMC6114981/

4. Ip W, Shao W, Song Z, Chen Z, Wheeler MB, Jin T. Liver-specific expression of dominant-negative transcription factor 7-like 2 causes progressive impairment in glucose homeostasis. Diabetes. 2015 Jun;64(6):1923–32.

5. Kim C-W, Addy C, Kusunoki J, Anderson NN, Deja S, Fu X, et al. Acetyl CoA Carboxylase Inhibition Reduces Hepatic Steatosis but Elevates Plasma Triglycerides in Mice and Humans: A Bedside to Bench Investigation. Cell Metabolism [Internet]. 2017 Aug 1 [cited 2021 Jun 14];26(2):394-406.e6. Available from: https://www.sciencedirect.com/science/article/pii/S1550413117304308

6. Hepatic De Novo Lipogenesis Is Present in Liver-Specific ACC1-Deficient Mice [Internet]. Molecular and Cellular Biology. [cited 2021 Jun 14]. Available from: https://journals.asm.org/doi/abs/10.1128/MCB.01122-06

7. Lee B, Fast AM, Zhu J, Cheng J-X, Buhman KK. Intestine-specific expression of acyl CoA:diacylglycerol acyltransferase 1 reverses resistance to diet-induced hepatic steatosis and obesity in Dgat1−/− mice. J Lipid Res [Internet]. 2010 Jul [cited 2021 Jun 14];51(7):1770–80. Available from: https://www.ncbi.nlm.nih.gov/pmc/articles/PMC2882751/

8. Reid BN, Ables GP, Otlivanchik OA, Schoiswohl G, Zechner R, Blaner WS, et al. Hepatic Overexpression of Hormone-sensitive Lipase and Adipose Triglyceride Lipase Promotes Fatty Acid Oxidation, Stimulates Direct Release of Free Fatty Acids, and Ameliorates Steatosis. J Biol Chem [Internet]. 2008 May 9 [cited 2021 Jun 14];283(19):13087–99. Available from: https://www.ncbi.nlm.nih.gov/pmc/articles/PMC2442319/

9. Ruiz-Villalba A, Mattiotti A, Gunst QD, Cano-Ballesteros S, van den Hoff MJB, Ruijter JM. Reference genes for gene expression studies in the mouse heart. Sci Rep [Internet]. 2017 Feb 2 [cited 2021 Jun 22];7(1):24. Available from: https://www.nature.com/articles/s41598-017-00043-9